JOURNAL OF GEOPHYSICAL RESEARCH, VOL. 103, NO. D13, PAGES 16,039-16,057, JULY 20, 1998

A global three-dimensional atmosphere-ocean model of methyl bromide distributions

J. M. Lee-Taylor, S. C. Doney, and G. P. Brasseur

National Center for Atmospheric Research, Boulder, Colorado

J.-F. Müller

Belgian Institute for Space Aeronomy, Brussels, Belgium

Abstract. A three-dimensional ocean-atmosphere model of the global methyl bromide budget is presented including an analysis of the temporally and spatially varying source and sink distributions. No correlation is found between oceanic net biological CH_3Br production, implied by surface water saturation anomaly observations, and oceanic variables such as surface chlorophyll and primary production; therefore model ocean fluxes are constrained directly by the saturation anomaly observations. The resulting diagnosed biological production rates imply net production in the tropics and subtropics and net consumption at high latitudes. Results from this semicoupled ocean-atmosphere model show substantial longitudinal variability in the atmospheric boundary layer CH_3Br concentrations with land-ocean contrasts of 1-6 ppt due to regional industrial and agricultural emissions on land and net fluxes into the ocean. Owing to an imbalance in current understanding of the global budget, our simulated mixing ratios of 3.5 to 6.5 ppt for the southern and northern hemispheres, respectively, are significantly lower than available measurements. Sensitivity studies reducing the ocean and soil surface sinks slightly improve the global mean CH_3Br concentration but increase the interhemispheric ratio further beyond that supported by observations. Accordingly, an apparent terrestrial missing source of 89 - 104 kT yr^{-1} is derived and applied to the model. This is of the same order as the sum of all other sources in the model (85 kT yr^{-1}). The hemispheric distribution of the missing source is explored, indicating that 50 - 70% of this source occurs in the southern hemisphere and is likely to be biased toward tropical regions. Modeled seasonal variability in the interhemispheric ratio at specific monitoring sites agrees well with observations. The model-predicted vertical gradient of CH_3Br through the troposphere and lower stratosphere is also presented.

1. Introduction

Since the discovery that industrially produced chlorine- and bromine-containing compounds are responsible for dramatic ozone depletion over Antarctica and, to a lesser extent over the Arctic and midlatitudes, the international community has made significant efforts to phase out these compounds and to develop less environmentally damaging alternatives. The 1997 Montreal Amendment to the Montreal Protocol [*United Nations Environment Programme (UNEP)*, 1997] stipulated that industrial production of methyl bromide in developed countries should be capped at 1991 levels, followed by a stepped phaseout and a total ban in 2005, while the U.S. Environmental Protection Agency (EPA) has prohibited import or production after the year 2000. With a mixing ratio near the tropopause of about 9 - 10 parts per trillion (ppt) or pmol mol^{-1}, methyl bromide contributed approximately 55% of the total organic bromine burden of the 1991 and 1996 stratosphere [*Daniel et al.*, 1996; *Schauffler et al.*, 1993a, 1998]. This proportion will likely increase in the short-term future as the mixing ratios of the bromine-containing Halons decline in response to an earlier cessation of industrial production than stipulated for methyl bromide. Bromine is estimated to be at least 40 times as efficient for stratospheric ozone destruction as chlorine on a molecule-for-molecule basis in the polar regions [*Solomon et al.*, 1992] and possibly 100 times more efficient in midlatitude regions. Thus it is important to understand fully the environmental interactions of methyl bromide, especially as its budget is significantly more complex than those of the other anthropogenic bromocarbons.

There are two main areas of uncertainty in our understanding of the role of methyl bromide in the environment. First, the fraction of global emissions of methyl bromide resulting from agricultural and industrial activity has a significant uncertainty margin. Second, current assessments of the global budget suggest that there is a substantial imbalance between the magnitudes of natural sources and sinks.

Figure 1 summarizes the currently known terms for the methyl bromide budget in the late 1980s and early 1990s. The total atmospheric burden of CH_3Br, 150 kT (box), is derived from observations of tropospheric mixing ratio: 11 - 12 ppt in the remote northern hemisphere with remote

Paper number 98JD00970.
0148-0227/98/98JD-00970$09.00

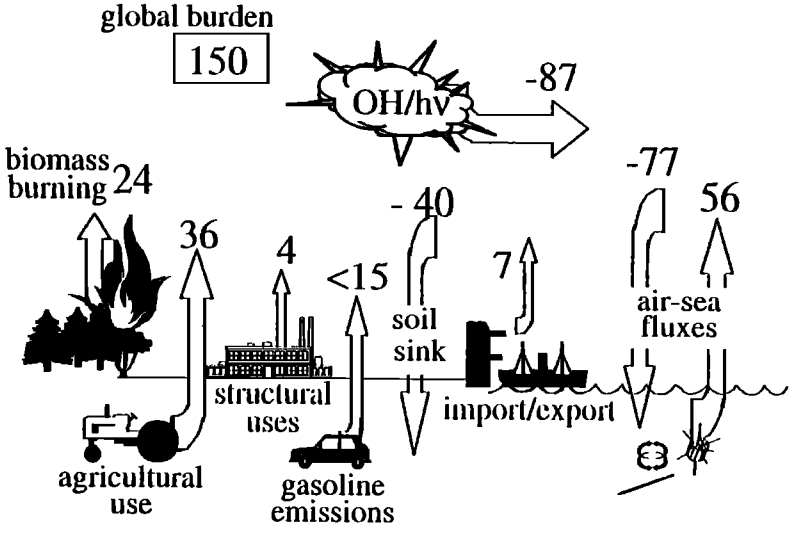

Figure 1. Summary of global atmospheric budget terms for methyl bromide for the late 1980s to early 1990s. Approximate fluxes are shown as kT yr^{-1}. Details and references are given in Table 1 and in the text.

southern hemisphere levels of 8 - 10 ppt [*Blake et al.*, 1993; *Schauffler et al.*, 1993b; *Khalil et al.*, 1993; *Lobert et al.*, 1995, 1996]. Ninety-five percent of the total atmospheric burden of CH_3Br is located in the troposphere [*Lal et al.*, 1994]. Chemical destruction by OH within the troposphere forms a major loss pathway for methyl bromide. This reaction occurs with a lifetime of 1.8 years [*Butler and Rodriguez*, 1996, after *Prinn et al.*, 1995], and the global lifetime with respect to stratospheric loss and photolysis is approximately 35 years [*Prather*, 1995], giving a net sink of 87 kT yr^{-1} within the atmosphere. An atmospheric CH_3Br trend of 0.15±0.1 ppt y^{-1} was calculated for 1978-1992 by *Khalil et al.* [1993]. This value has a large relative uncertainty; unfortunately, no other study has been of sufficient duration to unambiguously identify a trend.

The main technological source of methyl bromide is from its use as an agricultural fumigant. Its efficacy against a wide variety of weeds, pests, and microorganisms gives it wide application in pretreatment of soils before planting. Applications are also found in sterilization of produce for international trade and in structural pest control [*Anderson and Lee-Bapty*, 1992]. *Manö and Andreae* [1994] showed that methyl bromide is produced in significant quantities by biomass burning. There has been recent revision of understanding of the role of the oceans in the budget of methyl bromide. Originally, measurements of widespread supersaturations of methyl bromide in oceanic waters [*Singh et al.*, 1983; *Khalil et al.*, 1993] suggested a significant oceanic source, suspected to be biologically mediated. *Lobert et al.* [1995], however, demonstrated that analytical techniques used in previous studies could potentially indicate anomalously high oceanic concentrations. They found extensive undersaturation of methyl bromide in the eastern Pacific open ocean, contrasting with only limited areas of supersaturation, and inferred a small net global sink. Subsequently, *Moore and Webb* [1996] and *Lobert et al.* [1997] found even greater degrees of undersaturation in high-latitude oceanic waters and suggested net destruction (assumed to be biologically mediated) rather than net production in these regions, reinforcing the notion of the oceans as a net sink for CH_3Br. In addition to oceanic and atmospheric sinks, there appears to be significant loss to land surfaces. The only published quantitative study, that of *Shorter et al.* [1995], suggests a global net sink of 42 kT yr^{-1} due to soils. There is also evidence of rapid uptake by various types of plant leaves [*Jeffers and Wolfe*, 1998]. Unfortunately, a global estimate of the magnitude of this process is not currently available. The budget outlined here does not balance: sinks outweigh sources by a quantity of the same order as the estimate of total anthropogenic sources.

Because of the interdependence of the oceanic and atmospheric reservoirs of methyl bromide, it appears that coupled ocean-atmosphere models are likely to be the most successful approach for representing the behavior of methyl bromide in the global environment. This paper presents such a study, using the three-dimensional (3-D) global tropospheric model IMAGES [*Müller and Brasseur*, 1995] coupled with a simple global oceanic mixed-layer model. Given the imbalance in current understanding of the budget, the present-day atmospheric burden cannot be accurately simulated. However, valuable constraints are obtained for any further source terms proposed to close the CH_3Br budget. A 3-D model study allows explicit representation of longitudinal structure and land-ocean differences, which cannot be simulated in a 2-D study. Longitudinal structure can influence characterization of interhemispheric ratios (IHRs), which are often used to constrain estimates of the total anthropogenic contribution to the global budget [e.g., *Reeves and Penkett*, 1993; *Singh and Kanakidou*, 1993; *Wingenter et al.*, 1998]. Three-dimensional model simulations allow us to quantify seasonal changes in IHR as well as variations dependent upon the locations between which IHR is evaluated. Substantial land-sea contrasts in atmospheric surface CH_3Br concentrations may also influence computed source/sink terms.

The following two sections (2 and 3) describe the coupled model system, including a detailed presentation of the source and sink parameterizations used. The oceanic CH_3Br budget, including the net biological production/consumption rates and oceanic lifetime, is evaluated in section 3. Model

simulations and sensitivity study results are discussed with reference to observations in section 4. We construct an estimate of present-day sink magnitudes and diagnose a missing source term, which is then added to our baseline model. Further sensitivity studies, constrained by observations, allow us to place rough constraints on the characteristics of this source term. Section 5 summarizes the main conclusions.

2. The Atmospheric Model

2.1. Model Description

The Intermediate Model of Global Evolution of Species (IMAGES) is a global 3-D chemical transport model of the lower atmosphere with 5° × 5° resolution in the horizontal plane and 25 vertical σ-coordinate levels, extending to a pressure level of 50 mbar (approximately 20 km altitude). Tracer transport is driven by monthly averaged winds from an European Centre for Medium-Range Weather Forecasts (ECMWF) analysis. The effect of wind variability is taken into account as a mixing process, with diffusion coefficients calculated from the ECMWF variances. Deep convection in cumulo-nimbus clouds and planetary boundary layer mixing are also parameterized. The chemistry of approximately 55 species is considered, including the oxidation of several prominent nonmethane hydrocarbons (NMHCs). The photodissociation rates are interpolated from a predefined array of photodissociation coefficients [*Müller and Brasseur*, 1995]. The surface emissions of gases are based on the inventory by *Müller* [1992], with further modifications described by *Müller and Brasseur* [1995] and *Granier et al.* [1996]. A full description of the model, as well as a comparison of the model results with observations for O_3, CH_4, CO, NO, and HNO_3, is presented by *Müller and Brasseur* [1995].

The version of the model used in the present study contains a number of refinements over that described by *Müller and Brasseur* [1995]. Some of these changes have an important impact on the oxidation capacity of the atmosphere calculated by the model. First, the chemical rate constants and photodissociation parameters for CH_3Br are updated [*De More et al.*, 1994], and the photodissociation coefficient array is now calculated using the discrete ordinate method of *Stamnes et al.* [1988]. The washout parameterization has been refined, leading to higher lifetimes for soluble species. The boundary condition at the top of the model domain, which was zero flux in the work by *Müller and Brasseur* [1995] (except for HNO_3 and O_3), is now a "constant gradient" condition which allows non-zero fluxes in either direction at the domain boundary. The oceanic source of CO has been reduced from 165 Tg yr^{-1} [*Müller and Brasseur*, 1995] to 20 Tg yr^{-1} [*Bates et al.*, 1995], and the biomass burning emissions are taken from a new database, as described by *Granier et al.* [1996]. Finally, the biogenic NMHC emissions from *Müller* [1992] have been multiplied by a factor of 2, amounting to a total of about 1000 Tg y^{-1} globally [*Guenther et al.*, 1995]. These changes bring the methane global lifetime to 8.7 years, down from 11 years [*Müller and Brasseur*, 1995]. (The currently accepted observationally based value is 8.9 years [*Prinn et al.*, 1995]).

The major chemical loss mechanism for methyl bromide in the troposphere is reaction with OH. The global lifetime for methyl chloroform calculated by IMAGES, 4.4 years, is within the range of lifetimes calculated by *Prinn et al.* [1995] (4.6±0.3 years), showing that the OH distribution calculated within this version of the model gives results consistent with observations. Tropospheric photolysis of methyl bromide is of only minor importance as is reaction with $O(^1D)$. Rate expressions included in the model for these processes and the OH reaction are taken from *DeMore et al.* [1994].

The model is generally run with a 1-day time step for 6 years from an initialization of a selected globally uniform CH_3Br mixing ratio. Input figures and environmental parameters are monthly averages. The diurnal photochemistry cycle is set by averaging over 1 day with a 1-hour time step at the start of each month. By the final year of the simulation, the annual rate of change of CH_3Br mixing ratio is generally ±1% or less.

2.2. Land-Based Sources and Sinks

The currently known land-based sources and sinks of methyl bromide are quantified with widely varying degrees of uncertainty. Table 1 summarizes the values employed in the present study, together with the range of values currently presented in the literature. The following sections discuss the assumptions made here in parameterizing these sources and sinks. Plate 1 shows the seasonal cycle of emissions from each anthropogenic source for each hemisphere. Oceanic processes will be dealt with in section 3.

2.2.1. Agro-industrial sources. Industrial production for a variety of applications is probably the best quantified part of the methyl bromide global budget. We have adopted the sales figures for the year 1992 in the report of the *Methyl Bromide Global Coalition (MBGC)* [1994], which are listed for "reporting companies" by end use and by geographical region. These figures are estimated to account for over 95%

Table 1. Surface-Based Emissions and Sinks of Methyl Bromide by Hemisphere Incorporated Into the Model

Description	North	South	Total	Literature Range[a]
Soil fumigation (pre-planting)	33.5	2.5	36.0	16 - 52 [b,c]
Biomass burning	15.9	7.6	23.5	9 - 50 [d]
Gasoline-related	14.0	1.0	15.0	0.5 - 22 [e,l]
Quarantine uses	6.3	0.8	7.1	≤ 7.6 [b,g]
Structural uses	1.9	0.1	2.0	≥ 1.8 [b]
Inadvertent emission	1.8	0	1.8	≤ 2.1 [f,h]
Ocean source	(23.5)	(32.5)	56[i]	
Oceanic sink	(-32.3)	(-44.7)	-77[i]	
Soil sink	-26.8	-13.5	-40.3	-10 to -74 [j]

Values are in units of kT yr^{-1}.

[a] References are more fully explained with the description of each source or sink, in the text.

[b] *MBGC* [1994].

[c] *Rolston, and Glauz* [1982], *Yagi et al.* [1993].

[d] *Manö, and, andreae* [1994].

[e] J. Baker et al. and T. Chen et al. (manuscripts in preparation, 1998).

[f] *Penkett* [1995].

[g] *Anderson and Lee-Bapty* [1992].

[h] *MBIP/CMA* [1992].

[i] Global values of *Yvon-Lewis, and Butler* [1997]. Parentheses show assumed hemispheric distribution, proportional to ocean surface area. (Flux amounts vary in the present study.)

[j] *Shorter et al.* [1995]. Values correspond to a uniform global mixing ratio of 11 ppt.

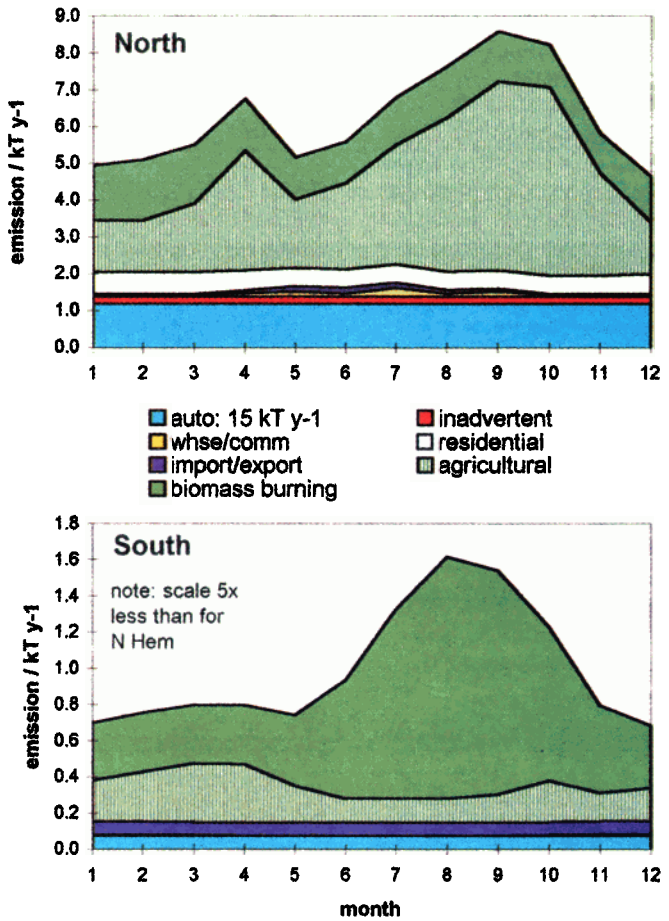

Plate 1. Seasonal cycles prescribed for land-based sources of methyl bromide (kT yr^{-1}). From the bottom (northern hemisphere), emissions are from automobile exhausts, inadvertent emission, warehouse/commercial structural use, residential structural use, import/export fumigation, agricultural use, and biomass burning. Inadvertent emissions and release from structural uses are virtually neglible in the southern hemisphere. Note the different *y* axis scales.

of global sales. Also utilized are the 1990 estimates for total sales in China, India, and the countries of the former USSR from the same report, the most recent year for which estimates are available. The modeled distribution of these sales, geographically and seasonally, is considered on a source-by-source basis, as is the proportion which is emitted into the environment.

Fumigation of soils before planting is the largest single use of methyl bromide worldwide, accounting for just over 80% of the *MBGC* [1994] sales figures for 1992. A broad-spectrum biocide, it is mainly utilized in the cultivation of high-value, intensively grown crops such as tomatoes, strawberries, and eggplant (aubergine) as well as ornamental plants, tobacco, and turf [*Anderson and Lee-Bapty*, 1992]. Assuming that agricultural use accounts for all sales in China, India, and the former USSR, the 1992 global total annual sales for agricultural fumigation usage amounts to 59.9 kT.

The proportion of methyl bromide applied to soils which eventually reaches the atmosphere is not well characterized. CH_3Br retention can vary widely in response to factors such as soil moisture, acidity and organic content as well as depth of injection and the presence and efficiency of plastic sheeting ("tarp") used to cover the treated area to retain the fumigant within the soil [*Yagi et al.*, 1993, 1995]. Re-deposition immediately downwind of the treated area is also possible [*Seiber et al.*, 1995] and is assumed in this study to be accounted for by the general description of the soil sink (section 2.2.3). Overall, estimates of retention range between 27% with inefficient tarping [*Rolston and Glauz*, 1982] and 87% [*Yagi et al.*, 1993] of quantity applied. *Gan et al.* [1994] suggest that "substantial" degradation of CH_3Br within the soil profile is unlikely and that fumigant applied may readily diffuse out of the soil. They attribute most of the within-soil loss to dissolution in soil waters, a conclusion consistent with the finding of *Ellis et al.* [1995] that plants grown on fumigated soils contain elevated levels of bromine. We assume a midrange value of 60% emission from agricultural sources in this study, making no attempt to account for regional variations in retention rates.

Emissions are distributed globally by weighting the sales within each region [*MBGC*, 1994]; first by country, according to the total weight of selected crops produced [*Anderson and Lee-Bapty*, 1992; *Food and Agriculture Organization*, 1990], and then within countries according to the distribution of cultivated land [*Müller*, 1992; after *Olson et al.*, 1983, 1985]. Bias within large countries toward grain-producing regions (where methyl bromide is not used) is lessened by restricting modeled usage to regions with an annual mean temperature above 9°C. Within the United States, government statistics [*U.S. Department of Agriculture*, 1991] suggest that the main centers of use are in California and Florida with more minor usage in the southeast. Hence, all sales for the United States are distributed in the model among California, Florida, and the remaining southeastern states in the proportion 6:3:1. Seasonality of use is modeled assuming two main seasons: a spring pre-planting application and a more substantial application through late summer and fall, between harvesting and planting of a second (or winter) crop. The fall peak is corroborated by the September timing of the fumigation monitoring work of *Yagi et al.* [1993] and by the observation of elevated atmospheric concentrations of CH_3Br off the California coast in October by *Miller and Weiss* [1995]. The annual mean distribution of all modeled agro-industrial sources is shown in Plate 2a.

Post-harvest fumigation, also known as quarantine or commodity fumigation, is the second main commercial application for CH_3Br, accounting for 9.56 kT yr^{-1} or 13% of the 1992 reporting companies' production [*MBGC*, 1994]. A wide range of trade commodities, including perishable and dried foods and other natural products, is treated either before international shipment or upon reaching the port of destination [*Anderson and Lee-Bapty*, 1992]. This use is modeled by distributing the sales figures for each region [*MBGC*, 1994] evenly among the major grain- and container-handling ports identified by *Couper* [1983] in that region. Usage is assumed to be constant year-round. Emissions were set at 75% of sales, considering the rough maximum estimate by *Anderson and Lee-Bapty* [1992] of 80% total emission.

Structural fumigation uses, both commercial and residential, together account for under 3% of reported sales, or less than 2 kT yr^{-1} [*MBGC*, 1994]. Residential CH_3Br applications are distributed spatially in proportion to the agricultural CH_3Br emission distribution within each region, assuming house and field pests to have similar distributions.

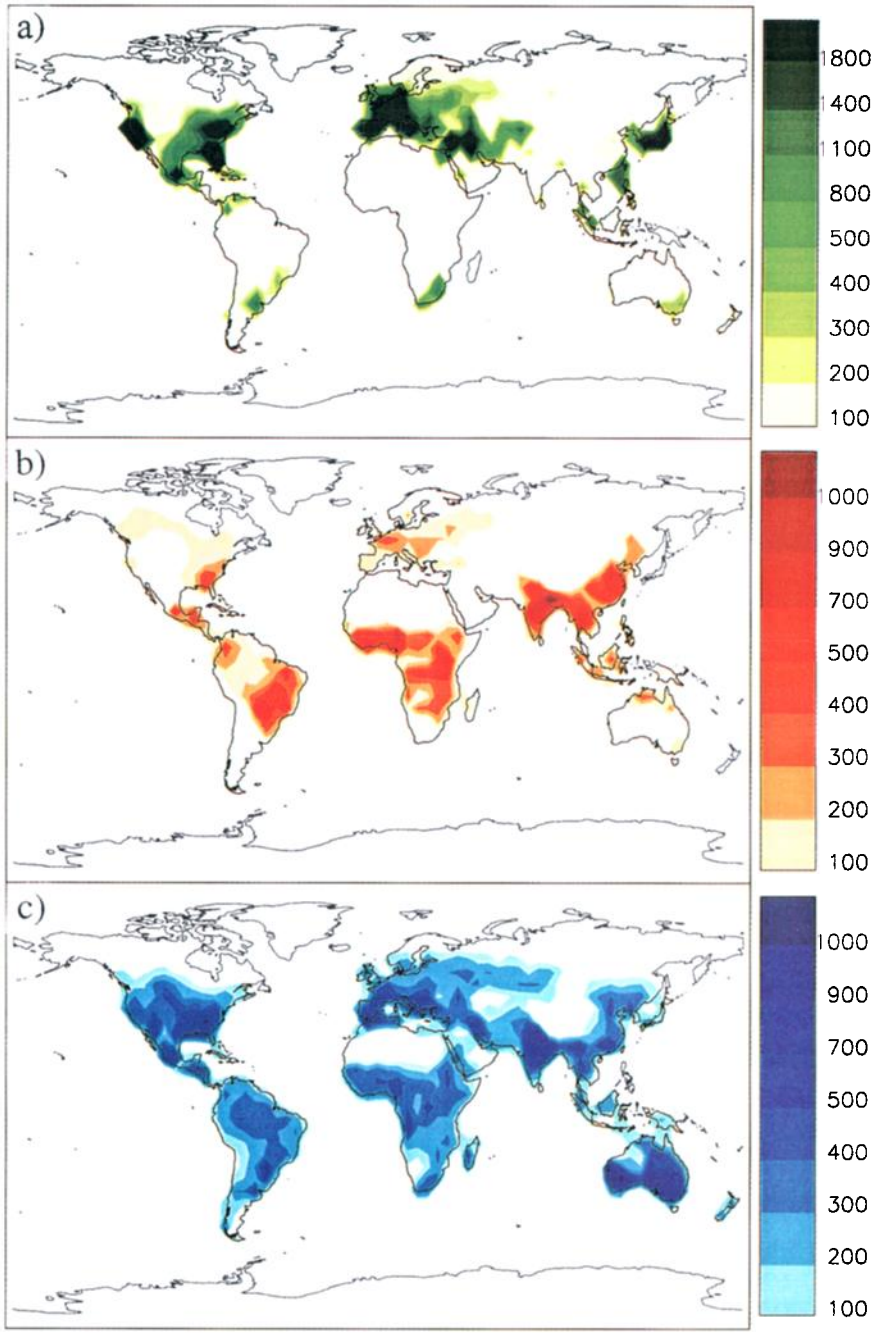

Plate 2. Annual mean surface CH_3Br source and sink distributions used in the model (g km^{-2} yr^{-1}): (a) agro-industrial sources, (b) biomass burning sources, (c) soil sink for a uniform 11 ppt atmospheric mixing ratio. Values less than 100 g km^{-2} yr^{-1} are not shown and scales are nonlinear, for clarity.

An emission rate of 100% is assigned, released year-round from tropical regions and in summer only, elsewhere. For warehouse/commercial fumigation applications, 100% release is likewise assigned, with 2 to 3 times greater release in summer, due to increased risk of pest infestation, than in winter. Distribution is weighted by the energy consumption distribution of *Müller* [1992], used here as an indicator of commercial activity.

Penkett [1995] suggests global inadvertent production and fugitive emissions of 2.1 kT yr^{-1}, reflecting emissions from all sections of the industry equivalent to 3.1% of the annual mean total CH_3Br sales from 1984 to 1990 [*Methyl Bromide Industry Panel/Chemical Manufacturers Association*, 1992]. An estimate of inadvertent emissions was made in this study of 1.8 kT yr^{-1}, 2.5% of the total 1992 CH_3Br sales figure [*MBGC*, 1994]. These emissions are distributed within the regions reporting sales of chemical intermediates by scaling to the energy consumption distribution of *Müller* [1992] and assuming no seasonal variability. While the methyl bromide produced for industrial use as chemical intermediates is

intended to be converted completely into other compounds and not emitted, this index gives a means of estimating a distribution of general inadvertent industrial methyl bromide production.

Gasoline-related emissions of methyl bromide are the subject of considerable uncertainty. CH_3Br is a by-product of the combustion in vehicle engines of ethylene dibromide, a component of leaded gasoline. Estimates of the global source strength of methyl bromide due to this process range from 0.5 to 22 kT yr^{-1}. In this study we employed the higher of the two "best estimate" values quoted by *Penkett* [1995] (after M. Speigelstein, personal communication, 1994), 15 kT yr^{-1}, which is equivalent to 40% of the agricultural emission assumed here. These emissions are distributed geographically according to global oil consumption [*Müller*, 1992] and with no seasonal cycle. This treatment likely overestimates the relative contribution of the United States to the global source, as a lower proportion of leaded fuel is used there than in many other parts of the world. In addition, recent work by J. Baker et al. and T. Chen et al. (manuscripts in preparation, 1998) suggests that a lower global estimate of less than 5 kT yr^{-1} might be more appropriate. This value is used in the current work for evaluation of the global missing source.

2.2.2. Biomass burning. Biomass burning is a significant, though poorly constrained, source of methyl bromide. Largely induced by human activity, these by-product emissions are nonetheless virtually impossible to regulate, in contrast to the deliberate usage of CH_3Br as an agro-industrial chemical. *Manö and Andreae* [1994] estimate a global source range of 9 - 37 kT yr^{-1} or 22 - 50 kT yr^{-1}, depending whether CH_3Br emissions are calculated with reference to CO_2 or CH_3Cl, respectively. *Andreae et al.* [1996] calculate a fourfold lower value of the $\Delta CH_3Br/\Delta CO_2$ emission ratio from savanna regions than do *Manö and Andreae* [1994], based on a larger number of samples, and estimate a global source of 24 kT yr^{-1}. Similarly, *Blake and Rowland* [1995] report a global estimated source strength of 15 - 30 kT yr^{-1} from CH_3Br emission ratios to methane.

Biomass burning is distributed in the IMAGES model as described by *Granier et al.* [1996] (see Plate 2b). The distribution distinguishes between burning of fuelwood and agricultural wastes as well as between forest and savanna grassland burning. CH_3Br emissions are estimated by applying emission factors to the modeled biomass burning derived CO_2 emissions. *Manö and Andreae* [1994] show that CO_2 is not a perfect analog for CH_3Br, since the ratio of emissions of the two compounds differs between flaming and smoldering fire phases. Correspondence is, however, closer than if ratios to CO are used. We extend their $\Delta CH_3Br/\Delta CO_2$ emission ratio of 1.3×10^{-6} quoted for boreal forests to all forested areas, noting that forest burning mainly takes place in tropical regions, for which we are unaware of any published forest emission ratio estimates. We assume that fuelwood and agricultural burning types also emit CH_3Br and CO_2 in the same ratio, analogous to the NO_x emission pattern from the same sources within the IMAGES model. The latter two burning types comprise 22% and 12% of the biomass burning CO_2 emissions inventory,respectively, while forests make up 27% and savanna and grassland account for 40%. Using the *Manö and Andreae* [1994] savanna $CH_3Br/\Delta CO_2$ emission ratio of 4.6×10^{-7}, the total global CH_3Br source strength from biomass burning is 23.4 kT yr^{-1}, comparable to the mean source value (24 kT yr^{-1}) from the studies mentioned above. When the savanna emission ratio is reduced to 1.1×10^{-7} [*Andreae at al.*, 1996], the total source strength drops to 20 kT yr^{-1}. As biomass burning occurs, to a great extent, in tropical regions, uncertainties in this source might be expected to have minimal effect on the magnitude of the interhemispheric gradient of CH_3Br.

2.2.3. Soil sink parameterization. In addition to losses of CH_3Br to soil within the immediate vicinity of agricultural application, it appears that uptake by soils may comprise a significant sink worldwide. Chemical mechanisms for the destruction in soils of ppm-level CH_3Br concentrations have been identified [*Gan et al.*,1994], while microbial activity has been implicated in soil uptake of CH_3Br over a wide range of mixing ratios [*Oremland et al.*, 1995; *Shorter et al.*, 1995].

We use here the results of the laboratory and field studies of *Shorter et al.* [1995], which were performed at ambient-level CH_3Br concentrations on five different types of soil from different climatic regions. *Shorter et al.* [1995] extrapolated the resulting daily flux rates globally following the vegetation distribution of *Born et al.* [1990] and assumed that no contribution to CH_3Br uptake is made by swampy, boggy or tundra areas, including rice paddies. Our distribution uses the vegetation classification index of *Olson et al.* [1983, 1985] and similarly excludes waterlogged or frozen areas. Seasonality is accounted for in the assessment of *Shorter et al.* [1995] by assigning to each of their five biome types an "active season" during which the uptake rate is assumed to be constant, and zero during the remainder of the year. We assume that the microbially mediated uptake is temperature dependent and apply the following general microbial activity / soil temperature relationship, a composite of the results of *Holland et al.* [1995] and *Cleveland et al.* [1993] (E. Holland, personal communication, 1996):

$$y = [1 + \exp(kT)] / [1 + \exp(kT_0)] \quad (1)$$

where y is the uptake scaling factor due to microbial activity and $k = 0.057$. T represents monthly mean soil surface temperature (°C), and T_0= 25°C, the temperature at which the soil uptake rate constants of *Shorter et al.* [1995] were assessed. Consequently, modeled CH_3Br uptake is reduced at lower temperatures, with an additional constraint imposed such that microbial activity (and hence uptake) ceases when $T \leq 0$°C.

Although use of the *Olson et al.* [1983, 1985] vegetation index increases the soil area under consideration by one-third over that considered by *Shorter et al.* [1995], we evaluate an annual sink for a prescribed 11 ppt atmospheric CH_3Br concentration of 40.3 Gg yr^{-1}, almost identical to their value of 42 ±32 Gg yr^{-1}. The uncertainty of the sink magnitude should be considered to be of a similar order in the present study. The latitudinal distribution of the calculated sink is also different between the two studies: *Shorter et al.* [1995] calculated that the tropical regions should account for only 15% of the total loss, with temperate and cultivated regions contributing 81% and boreal regions making up the rest. Tropical losses in the present study are 31% of total loss and temperate and cultivated regions account for 66%, while the ratio of total losses between the northern and southern hemispheres is 2:1. The total annual soil uptake distribution for a constant atmospheric CH_3Br concentration of 11 ppt is shown in Plate 2c. In our model, the rate of CH_3Br uptake

by soils is calculated as a deposition velocity rather than as a net flux, with the result that the instantaneous flux is directly proportional to the overlying atmospheric concentration of CH_3Br.

3. The Model Ocean

3.1. Theoretical Approach

Whether the global ocean is a net source or net sink of methyl bromide is the subject of recent debate (see the discussion in the Introduction). Physical-chemical destruction processes (hydrolysis, chloride ion exchange and downward mixing into the thermocline) are relatively well known and are detailed in section 3.3. Biological processes are also implicated in CH_3Br cycling but are not yet well characterized. Though ice algae [*Sturges et al.*, 1993] and several cold-water diatoms [*Scarratt and Moore*, 1995] have been shown to produce CH_3Br in varying amounts and seaweeds are known to produce assorted halomethanes [e.g. *Gschwend et al.*, 1985], organism studies have so far yielded no direct relationship of in situ CH_3Br production or destruction to organism growth rate or to any external factor which can account for the quantities observed.

An alternative approach is to search for a net relationship between CH_3Br and bulk properties of the marine environment. The chlorophyll-based production extrapolations of *Anbar et al.* [1996] and *Pilinis et al.* [1996] give large estimates of methyl bromide oceanic source at high latitudes due to the assumption that net biological oceanic CH_3Br production (P_o) could be described as a function of chlorophyll, which increases at high latitudes. (P_o includes biologically mediated destruction; the subscript *o* denotes an oceanic quantity). The much slower rate of chemical destruction of methyl bromide [*King et al.*, 1995] in colder waters than at warmer low latitudes would further enhance the seawater concentrations due to high implied P_o in these regions. We find, however, using a method similar to that of *Anbar et al.* [1996], that not even oceanic primary production (calculated from ocean color data and photosynthetically available radiative energy, [*Antoine et al.*, 1996]) shows any significant relationship with P_o inferred from the oceanic and atmospheric transect data of *Lobert et al.* [1995] (Figure 2). Thus it appears that no one equation can realistically represent a relationship between globally measurable biomass attributes and P_o.

The 40 - 50% undersaturations in the Labrador Sea reported by *Moore and Webb* [1996] and the >35% undersaturations reported by *Lobert et al.* [1997] in the Southern Ocean are observational evidence that in situ CH_3Br production and chlorophyll have no simple relationship and further suggest that destruction by unknown processes, possibly biologically mediated, outweighs production at high latitudes.

In the absence of a reliable method of representing net P_o on the global scale in order to derive the air-sea exchange of methyl bromide, we instead extrapolate the saturation anomaly measurements of *Lobert et al.* [1995, 1996, 1997] and *Moore and Webb* [1996]. Figure 3a shows a best fit latitude-dependent function to a sampled subset of the data identified by those previous authors as having "open ocean" characteristics. The data set represents all four seasons except at high latitudes, where only summer and fall cruises apply. Our function,

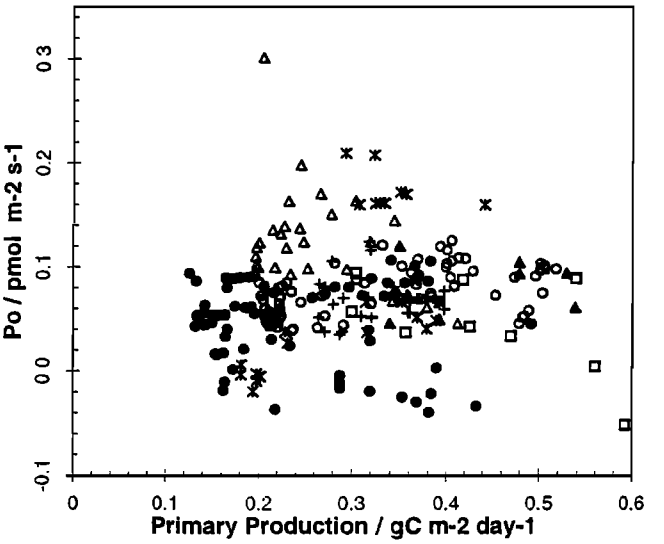

Figure 2. In situ production of oceanic methyl bromide implied by mass balance assuming steady state, from the saturation and SST data of *Lobert et al.* [1995], plotted against oceanic primary production [*Antoine et al.*,1996]. Regional classifications are given by *Lobert et al.* [1995]: solid symbols, northern hemisphere, winter; open symbols, southern hemisphere, summer; circles, open ocean; triangles, coastal waters; squares, inland passage; crosses, stars and plus signs denote various equatorial regions. We find no significant correlation in any region or season.

$$\text{saturation anomaly (\%)} = 29 \times \cos\theta - 50 \qquad (2)$$

with latitude denoted by θ, is applied globally so that any individual location is assigned a year-round constant saturation anomaly, representative of general open ocean conditions, from which the oceanic concentration and hence the net oceanic flux are derived. Equation (2) is an empirical tool used to simulate general oceanic conditions rather than being an exhaustive extrapolation of the rather variable observational data. The basic tendencies of the open ocean to be significantly undersaturated in CH_3Br and of polar waters to be highly undersaturated are preserved, though local conditions may vary by up to ±25% saturation about our function. Seasonal lags in CH_3Br equilibration due to factors such as finite air-sea gas exchange rates, advection or mixing are not compensated for in our model since the proxy CFC-11 data are not available for all cases [see *Lobert et al.*, 1995]. Coastal regions, which tend to show supersaturations [*Lobert et al.*, 1995, 1996], and the more variable upwelling areas are neglected in this treatment.

3.2. General Parameterization

The ocean is represented by a slab mixed layer on a 2.8° × 2.8° grid. Physical properties are applied as monthly averages. Solubility of methyl bromide is governed by the Henry's law coefficient (*H*) for seawater calculated after *Elliott and Rowland* [1993]:

$$H\ (\text{l atm mol}^{-1}) = 22.4 \times 3.86\times10^{3} \exp[-2859/T(\text{K})] \qquad (3)$$

Hence the oceanic partial pressure of CH_3Br changes in response to sea surface temperature (SST), defined here by the climatology of *Shea et al.* [1990, 1992].

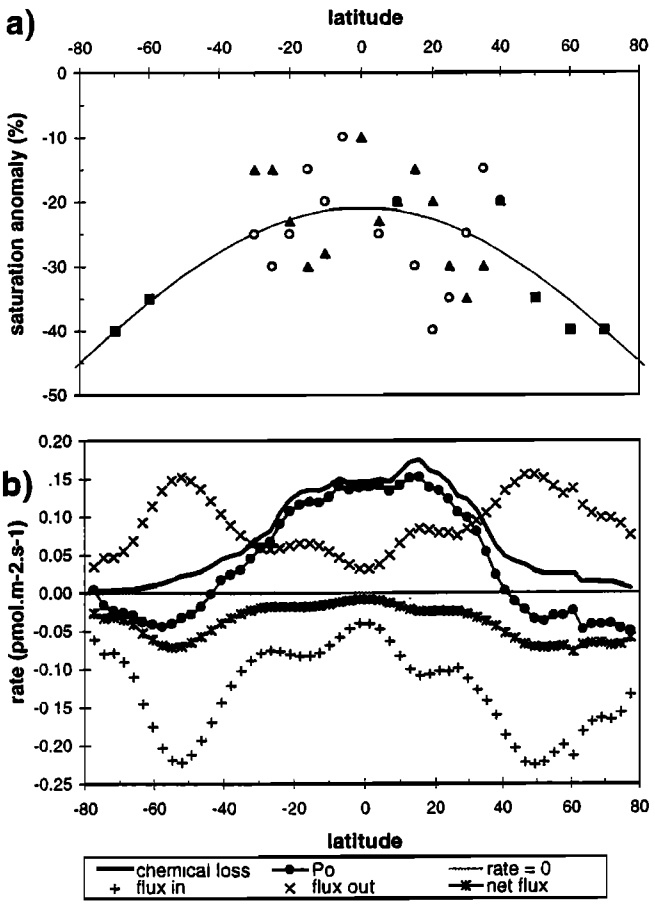

Figure 3. (a) Methyl bromide saturation anomaly function used in our model. Open circles show Pacific cruise data of *Lobert et al* [1995], solid triangles denote Atlantic cruise data, *Lobert et al.* [1996], and solid squares are a general representation of high-latitude saturation anomalies reported by *Moore, and Webb* [1996], and *Lobert et al* [1997]. The data were sampled at roughly 5° intervals to obtain an estimate of the tendency of saturation anomalies in open ocean waters. (b) Oceanic budget terms resulting from the above saturation anomaly distribution, calculated for our "best estimate" atmosphere. Rates are expressed as pmol m^{-2} s^{-1}. Air-sea fluxes are shown as negative for fluxes into the ocean so that P_o = chemical loss + net air-sea flux.

Ocean-atmosphere coupling is calculated every model time step, with the rates of flux into and out of the ocean being governed by the prevailing CH_3Br concentrations in the atmosphere and surface ocean, respectively, and interpolated in each direction between the different model grids. Since the saturation anomaly is constrained to remain constant, the oceanic partial pressure responds directly to atmospheric mixing ratio rather than being affected by fluxes. Mass is assumed to be instantaneously conserved by in situ losses and production. Air-sea exchange is parameterized using the relationship of *Wanninkhof* [1992] such that the transfer velocity for methyl bromide (k_{tCH3Br}) is calculated at each grid point by

$$k_{tCH3Br}\ (\mathrm{m\ s^{-1}}) = 0.39V^2\ (Sc_{CH3Br}/660)^{-1/2} / 3.6\times10^5 \quad (4)$$

where V is the monthly mean 10 m wind speed (m s^{-1}), averaged over the four year period 1985-1988 from the NCEP/NCAR reanalysis [*Kalnay et al.*, 1996]. Sc_{CH3Br} is the Schmidt number of methyl bromide (the kinematic viscosity of seawater divided by the viscosity of CH_3Br, a unitless quantity), expressed as a function of temperature (K) by *DeBruyn and Saltzman* [1997]:

$$Sc_{CH3Br} = 2004 - 93.5(\mathrm{T}-273) + 1.39(T-273)^2 \quad (5)$$

Ocean grid cells are isolated from each other; the only exchanges are those across the air-sea interface and through the thermocline. The in situ lifetime of CH_3Br is usually shorter than timescales of lateral exchange between grid boxes, so that, to a first approximation, lack of oceanic transport has little effect on large-scale atmospheric results. A monthly sea-ice distribution based on SST [*Shea et al.*, 1990, 1992] is applied, with the assumption that no net flux into or out of the ocean occurs where sea-ice is present. Monthly mixed-layer depths are computed from the *Levitus* [1982] climatology using a standard density criterion.

3.3. In Situ Destruction Terms

While not required in the modeling approach outlined above, in situ destruction rates are used explicitly in additional model simulations, designed to assess ocean-atmosphere interaction in the absence of biology or with a prescribed in situ net production climatology, and also for calculation of the lifetime of methyl bromide with respect to oceanic loss. In the abiological case the ocean is initialized by assuming it to be at equilibrium with the atmosphere and allowing evolution through chemical and flux processes. The net production climatology is derived by mass balance from the results of a simulation with fixed oceanic saturation anomaly, and a simulated present-day atmospheric mixing ratio distribution as discussed in section 4.2.

In situ chemical destruction of methyl bromide within the ocean (k_{chem}) is calculated from the total chemical loss rate expression of *King et al.* [1995] for all chemical loss processes, including hydrolysis and reaction with Cl^- :

$$k_{chem}\ (\mathrm{s^{-1}}) = 1.88\times10^{15}\ \exp[-14370/T(\mathrm{K})] \quad (6)$$

This quantity is evaluated at mixed layer temperature, T_{ml} (assumed to be equal to SST), and at thermocline temperature, T_{therm}, which is defined as 293 K (20°C) in the tropics [*Houghton*, 1991] and the lower of 288 K (15°C) [*Anbar et al.*, 1996] and SST elsewhere. Mixed-layer depth z, (meters) is defined by the monthly climatology of *Levitus* [1982]. Downward mixing and destruction in the thermocline

$$k_{mix}(\mathrm{s^{-1}}) = 1/z\ \sqrt{(D_t\ k_{chem})} \quad (7)$$

[*Yvon and Butler*, 1996; after *Johnson*, 1981; *Butler et al.*, 1991] is calculated at T_{therm} using D_t, the diffusivity through the thermocline, defined here as 1.0 cm^2 s^{-1}. (*Li et al.* [1984] give ocean-basin average values ranging widely from 0.4 to 9.5 cm^2 s^{-1}.) Entrainment or detrainment of CH_3Br due to mixed-layer depth changes is also considered as part of the mass balance system. CH_3Br is assumed to

be well mixed throughout the mixed layer with a diffusion-limited reduction to zero concentration below. A reduction in mixed-layer depth results in a loss of CH_3Br from the mixed layer equal to the burden over the range of the depth change, while an increase in z results in a dilution of the mixed-layer concentration, all other factors being equal.

Net production of methyl bromide within the ocean (P_o) is estimated from our simulated present-day atmospheric distribution (section 4.2) by constraining the oceanic CH_3Br saturation anomaly as in equation (2) and evaluating the budget terms described above. Mass balance yields net production (pmol m^{-2} s^{-1}) as

$$P_o = (k_{loss}C_o) + k_{tCH3Br}[C_o/z - X_a/H] + (\Delta C_o - E)/\Delta t \quad (8)$$

where $k_{loss}(s^{-1})$ is the sum of k_{chem} and k_{mix} and is generally dominated by k_{chem}, C_o(pmol m^{-2}) is the oceanic mixed-layer burden of CH_3Br, X_a (patm) is the atmospheric partial pressure, E(pmol.m^{-2}) represents monthly entrainment or detrainment and Δt is equal to 1 month. Resulting production rates are shown as annual zonal means in Figure 3b together with the corresponding flux and in situ degradation terms. These results give a vertically integrated P_o that is negative everywhere poleward of 40° and reaches a positive maximum in the tropics (Figure 3b). Total annual P_o in this scheme is estimated at 66 - 69 kT yr^{-1}, balancing a net flux of 29 - 32 kT yr^{-1} into the ocean and in situ physical-chemical losses of 93 - 101 kT yr^{-1}, including 4 - 5 kT yr^{-1} net loss to detrainment. (The ranges quoted here reflect the two different estimates of mixing ratio distribution described in section 4.2; no formal error is computed for the ocean budget due to the empirical nature of the parameterization.)

3.4. Lifetime Due to Oceanic Loss

The oceanic CH_3Br balance diagnosed by our model cannot be used directly to compute an atmospheric lifetime with respect to oceanic loss, since we do not separate the biological production and consumption terms, instead calculating only net production. Rather, the approach of *Yvon-Lewis and Butler* [1997] to the lifetime calculation is adopted. These authors use the high-latitude measurements of *Moore and Webb* [1996] and *Lobert et al.* [1997] and the coastal consumption rate data of *King and Saltzman* [1997] to estimate biological destruction, as distinct from production, and calculate a lifetime for methyl bromide, with respect to oceanic loss, of 1.8 - 1.9 years. We adopt their three different biological degradation rates (Table 2), corresponding to the three 30° latitude bands in each hemisphere, for addition to the net destruction rate, $k_{loss}(s^{-1})$. The CH_3Br lifetime with respect to oceanic loss is derived by factoring in transfer velocity, mixed-layer depth, and surface area A (m^2) (equation (9), [after *Yvon-Lewis and Butler*, 1997]:

$$\tau_{ocean}(s) = 1/\ 1.387\times10^{20}\,(k_{tCH3Br}\,A\,/H) \times [k_{loss}/(k_{loss} + k_{tCH3Br}/z)] \quad (9)$$

Note that lifetime is not directly proportional to the downward flux into the ocean, as some of the latter quantity may be re-emitted to the atmosphere rather than being removed by chemistry, biology, or mixing. The lifetime with respect to oceanic loss for a uniformly distributed atmospheric burden of methyl bromide was found to be 2.2 years, compared to the 1.8 - 1.9 years calculated by *Yvon-Lewis and Butler* [1997]. Adjustment of the wind speed to compensate for the lower global mean value used here (6.9 m s^{-1}: *Wanninkhof* [1992] assumes a value of 7.4 m s^{-1}) and consideration of an interhemispheric ratio of 1.3 reduces the calculated lifetime of CH_3Br with respect to oceanic loss to 2.1 years.

Table 2. Oceanic Biological CH_3Br Degradation Rates of *Yvon-Lewis and Butler* [1997] (Their Case 6)

Region	Loss rate d^{-1}	Loss rate s^{-1}
Tropical (30°N to 30°S)	0.090	1.04×10^{-6}
Temperate (30° to 60°N, and S)	0.071	8.22×10^{-7}
Polar (poleward of 60°N, and S)	0.052	1.02×10^{-7}

4. Results and Discussion

We begin our presentation of results in section 4.1, with simulations and sensitivity studies which use the sources and sinks already defined. Model results are evaluated with respect to atmospheric observations. An estimated present-day atmospheric distribution is derived in section 4.2 from the model results, enabling construction of a global budget for CH_3Br (section 4.3) and estimation of the magnitude of the global missing source of CH_3Br. Section 4.4 details further sensitivity studies incorporating the new estimated source into the global model and comparing the results with observations, enabling broad constraints to be placed on source partitioning between the hemispheres. Simulated seasonal cycles and altitude profiles at selected monitoring sites are also presented.

Model runs 1 - 4 include only those budget terms described previously, without attempting to balance the global budget of CH_3Br. The "base case" model scenario, run 1, includes all available source and sink estimates, with the oceanic saturation anomaly constrained by equation (2). Oceanic chemical or biological processes are not explicitly represented in this simulation. Two more simulations further investigate the effect of oceanic interactions. Run 2, the "no ocean" run, treats the ocean as a sealed, nondepositional surface (i.e., no ocean interactions are calculated). Run 3, "abiological ocean," has the ocean-atmosphere flux calculated by consideration of known oceanic chemical and physical loss processes and transfer velocity (section 3.3) but not of biological or unknown processes. In this scenario the ocean and atmosphere are truly coupled, since the evolution of each depends on the conditions of the other, whereas the other simulations may be considered to be "semicoupled" due to the imposition of an ocean saturation anomaly. The contribution of the soil sink is investigated by run 4, which uses the same ocean parameterization as in run 1 but with no deposition to soils considered. Runs 5 - 9 involve the addition of an additional net source, distributed over land surfaces and partitioned between the hemispheres in varying proportions. Run numbers and parameters are summarized in Table 3.

Table 3. Model Run Characteristics

Run	Characteristics
1	"Base case"; ocean constrained by fixed saturation anomaly
2	"No ocean"; no flux considered in or out of the ocean
3	"Abiological ocean"; oceanic flux driven by physical, and chemical factors only
4	"No soil sink"; ocean as Run 1, losses to soil not considered
5	Additional source of 94.4 kT yr^{-1}, distributed 50:50 between N and S hemispheres
6	"Tropical"; additional source of 94.4 kT yr^{-1}, between 17.5°N and S only
7	Gasoline emissions reduced to 5 kT yr^{-1}, additional source of 89.3 kT yr^{-1} distributed 50:50 between N and S hemispheres
8	As run 7, additional source distributed in ratio 40:60 N:S
9	As run 7, additional source distributed in ratio 30:70 N:S

Quote marks indicate additional short titles used in the text.

4.1. Modeling the Known Portions of the Budget

Annual mean global surface mixing ratios from run 1, the base case, and run 4, "no soils," are shown in Plate 3. In both cases, significant longitudinal variability is apparent, with surface mixing ratios over land-based source regions elevated by up to 12 ppt in the annual mean with respect to the oceanic "background" atmosphere. In the northern hemisphere the greatest enhancements coincide with major industrialized and agricultural source regions. The southern hemisphere is much more homogeneous, but enhancements of 1-2 ppt over South America and southern Africa are apparent, mainly in response to the biomass burning source. The continental enhancement is primarily isolated to the planetary boundary layer, ranging from 1 to 2 km in depth. These results are qualitatively supported by trajectory analyses of measurements of CH_3Br and correlations with other tracers by *Montzka et al.* [1994], which indicate that continentally derived air can routinely show mixing ratios elevated relative to those found in air associated with the marine boundary layer.

Annual zonal mean over-ocean mixing ratios for all four model runs are shown in Figure 4. Calculated mixing ratios are noticeably lower than atmospheric observations. Measurements give a northern hemisphere remote atmospheric mixing ratio of 11 - 12 ppt with remote southern hemisphere levels of 8 - 10 ppt [*Blake et al.*, 1993; *Schauffler et al.*, 1993b; *Khalil et al.*, 1993; *Lobert et al.*, 1995, 1996]. The base case (run 1) results give mean over-ocean mixing ratios of only 6.4 and 3.5 ppt for the northern and southern hemispheres respectively (Figure 4). The contrast between models and measurements reflects the fact that the known global budget is unbalanced at present-day

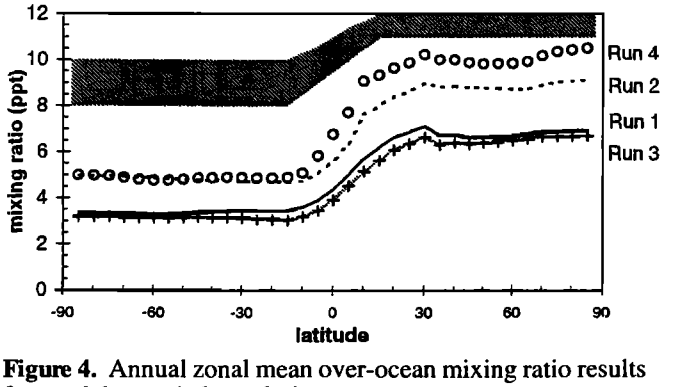

Figure 4. Annual zonal mean over-ocean mixing ratio results for model runs 1 through 4.

methyl bromide concentrations, with net sinks outweighing net sources. As already noted, ocean fluxes and the chemical and soil sinks in this simulation are proportional to the atmospheric mixing ratio: if these terms were included as calculated relative to observations, the model mixing ratio results would be driven much lower.

Measurements of atmospheric methyl bromide show a well-defined interhemispheric gradient with northern hemisphere mixing ratios exceeding those in the southern hemisphere by a factor of about 1.2 in the annual mean [*Wingenter et al.*, 1998]. Since the CH_3Br lifetime is comparable to the interhemispheric exchange time, net imbalances in sources and sinks between the hemispheres are implied. In all of our model results, there is also a pronounced north-south gradient which is steepest around the equator. The calculated interhemispheric ratio is substantially higher than the observationally based value, varying between 1.56 and 1.84 in the annual mean model results (Table 4, runs 1 - 4), due in part to the underestimation of the global budget.

Runs 2 and 4 explore the effects of simulating first the ocean and then the global soils as neutral surfaces, where uptake and emission are everywhere zero. This overemphasizes the effects of the uncertainty in each sink: even at the lower limits of observed uptake, the soil sink is nonzero [*Shorter et al.*, 1995] and the mean oceanic saturation anomaly is negative [*Lobert et al.*, 1995, 1996, 1997; *Moore and Webb*, 1996]. Alternatively, this approach is analogous to simulating an additional source with identical distribution and magnitude to each modeled net sink in turn. Results (Table 4, Figure 4) show little effect in longitudinal gradient. Additionally, while resulting mixing ratios increase from the base case over-ocean hemispheric means, neither scenario, nor both combined, can fully compensate for the modeled mixing ratio deficit, indicating that this deficit is not merely due to these sources of uncertainty.

The "abiological ocean" case, run 3, gives zonal mean over-ocean mixing ratios 3% to 12% lower than the base case, run 1 (Figure 4), and hemispheric means 5-6% lower (Table 4). The net air-sea flux is 29% higher than in run 1, though representing an increase of only 6% of the total modeled sink. The interhemispheric ratio assessed over the whole ocean remains the same, at 1.84 compared to the 1.83 calculated in the base case run (Table 4), despite significant latitudinal redistribution of the CH_3Br saturation anomaly and oceanic sink. In run 3, where known oceanic chemical-physical processes are explicitly represented and are driven by temperature dependence, CH_3Br shows intense

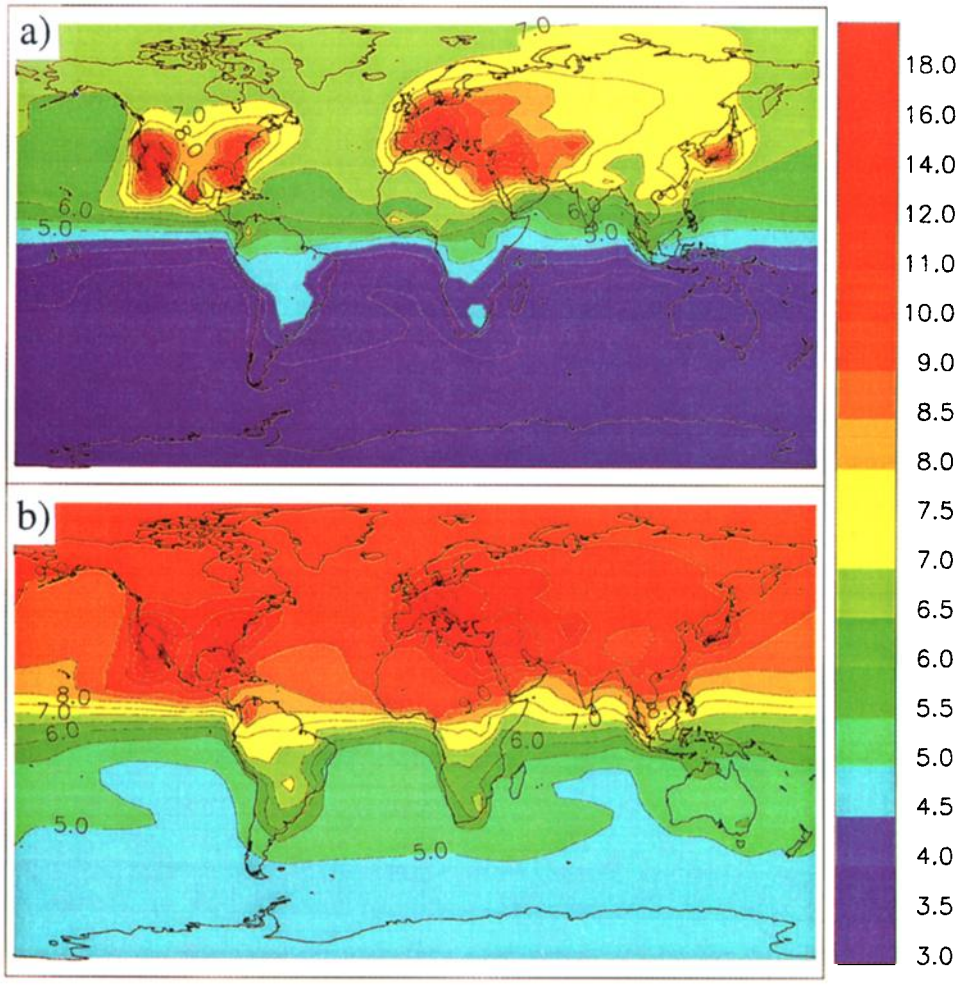

Plate 3. Annual mean mixing ratio results for (a) the "base case" model run 1 and (b) the model with no soil sink, run 4. The color scheme is the same for each panel. Removing the soil sink sharpens the land-sea mixing ratio gradients, and the equatorial mixing-ratio gradient by about 0.5 ppt but cannot raise modeled mixing ratios to observed values.

undersaturation (< -70%) in the tropical oceans and comparatively slight undersaturation (>-20%) at polar latitudes. This distribution is at odds with observational evidence [*Moore and Webb*, 1996; *Lobert et al.*, 1997] (Figure 3a), implying that additional in situ net production, whether via biological or unknown physical processes, has to be invoked at low latitudes and additional net destruction at high latitudes to realistically model oceanic CH_3Br.

4.2. Present-Day Atmosphere Estimation

Owing to the underestimation of mixing ratios in the base case results and the geographical and temporal sparsity of methyl bromide observations, a simulated atmospheric distribution (hereafter the "estimated present-day atmosphere") is constructed to enable the formulation of sink distributions for use in budget analysis calculations. A comparison (Figure 5) is made between the modeled monthly mean boundary layer mixing ratio from our base case simulation (run 1) and the atmospheric observations of *Lobert et al.* [1995, 1996] for model transects most representative of the observational shiptrack locations. The model results underrepresent the data by a mean of 5.5 ppt. We add this 5.5 ppt globally to the model results of run 1 to give a distribution estimated to be roughly equivalent to the present-day atmosphere. The resulting latitudinally weighted annual mean mixing ratio obtained is 9.1 ppt in the southern hemisphere and 12.4 ppt in the northern, with these values decreasing to 9.0 and 11.9 ppt if only oceanic regions are considered, yielding an over-ocean interhemispheric ratio of

Table 4. Modeled Interhemispheric Ratios and Latitude Weighted Hemispheric Mean Mixing Ratios

Run	Summary Title	AK/NZ	Whole Ocean	NH ppt	SH ppt
1	base case	1.95	1.83	6.4	3.5
2	no ocean	1.64	1.56	7.7	4.9
3	abiological ocean	1.99	1.84	6.1	3.3
4	no soil sink	1.78	1.70	8.8	5.2
5	50:50 N:S	1.47	1.38	12.0	8.7
6	tropical	1.35	1.33	11.4	8.5
7	50:50 N:S	1.42	1.36	10.9	8.0
8	40:60 N:S	1.32	1.27	10.6	8.3
9	30:70 N:S	1.22	1.19	10.3	8.7

AK/NZ refers to the ratio between modeled mixing ratios in Alaska, and New Zealand, as defined in the text. Hemispheric means are assessed as over-ocean values.

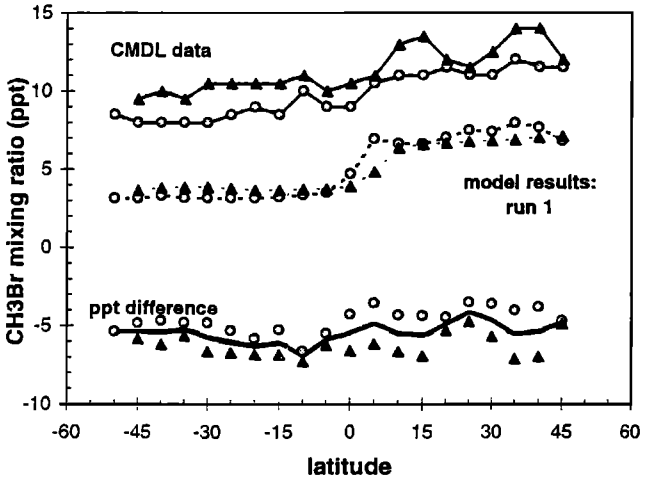

Figure 5. Comparison between our "base case" model results and atmospheric data. Open circles show Pacific points, and solid triangles are Atlantic points. Plotted are, from the top, the median sampled observations of *Lobert et al.* [1995, 1996] (joined by thin lines), and the model results along the cruise tracks (dashed lines). The lowest set of points is the difference (model minus data), and the heavy line is the mean difference.

1.32. (The term "over-ocean" indicates that only atmospheric mixing ratios calculated for oceanic regions are included in the analysis, for direct comparison to observational data). A second diagnosis is also performed based on the possibility that the Atlantic data might be elevated in places above background levels due to its proximity to continental sources. Addition of the mean difference between the Pacific data only and the model results, 4.7 ppt, yields over-ocean mixing ratios of 8.2 and 11.1 ppt in southern and northern hemispheres and an over-ocean interhemispheric ratio of 1.35.

4.3. Calculation of Global Budget Terms

The CH_3Br global budget for the estimated present-day atmosphere is shown in Table 5. The estimated present-day atmosphere is used to assess a "best estimate" for the oceanic, soil, and atmospheric sink distributions. The calculated soil sink is 41 - 44 kT yr^{-1}, compared to 40.3 kT yr^{-1} for a uniform 11 ppt atmosphere. The similarity with a uniform atmosphere suggests that the modeled steep CH_3Br gradients and elevated mixing ratios around source regions have only a small effect on the global soil sink. The oceans are also calculated to be a net sink of atmospheric CH_3Br, with a net flux of 29 - 32 kT yr^{-1} into the oceans; *Yvon-Lewis and Butler* [1997] derive a net uptake of 21 kT yr^{-1}. Because of our imposed saturation anomaly function (equation (2)), the modeled ocean flux is negative at all model ocean locations, while in reality localized regions may be a net source. *Lobert et al.* [1996] assign 10% of the global ocean to coastal zones and estimate a net emission from these areas of 1.5 kT yr^{-1} CH_3Br. If a similar constraint is imposed on our model ocean, the net oceanic uptake is reduced by 4 - 5 kT yr^{-1}. The ranges given here for the soil and ocean sinks reflect only the difference between the two estimated present-day distributions (run 1 augmented by 5.5 ppt and run 1 augmented by 4.7 ppt). It is inappropriate to attempt a statistical error analysis due to the highly approximate nature of the assumptions used in the present version of the model for both oceanic behavior and present-day surface mixing ratio.

Atmospheric loss of CH_3Br in our estimated present-day distribution totals 96 - 104 kT yr^{-1}, incorporating 89 - 97 kT yr^{-1} tropospheric loss due to OH chemistry and 6.8 - 7.4 kT yr^{-1} due to high-altitude photolysis and flux at the top boundary of the model (0.2 kT yr^{-1} loss). The model calculates 94.5 kT yr^{-1} loss due to OH if uniform CH_3Br mixing ratios throughout the southern hemisphere of 9.0 ppt and throughout the northern of 11.5 ppt are imposed.

We calculate a total atmospheric lifetime of 0.7 years for CH_3Br, based on lifetimes with respect to oceanic destruction (2.1 years), soil losses (3.7 years) and atmospheric chemistry (1.6 years). Our estimate of total atmospheric lifetime coincides with the most recent value calculated by the NOAA/CMDL group [*Yvon-Lewis and Butler,* 1997], 0.7 years with a range of 0.6 to 0.9 years. There has been a significant reduction in the calculated lifetime of CH_3Br in recent years: the consensus in the 1994 World Meteorological Organization (WMO) ozone assessment [*Penkett,* 1995] was that the lifetime was around 1.7 to 2.0 years. The discovery of the soil sink and publication of more comprehensive ocean measurements that imply a net oceanic sink have caused a downward revision of the net lifetime to the point where it is shorter than the timescale of interhemispheric exchange (typically, 1.1 - 1.2 years, [*Singh and Kanakidou,* 1993]).

We calculate a budget imbalance of 79 - 94 kT yr^{-1}, meaning that an additional net source of this size would be required to maintain the model atmosphere at the levels implied by Figure 5 with the source/sink formulation described in sections 2 and the oceanic saturation anomaly given by equation (2). The additional source required to balance the budget is at least as large as the sum of all sources currently incorporated into the model. We note that the additional postulated net source is unlikely to have a distribution proportional to that of the soil sink presented here, since our "no soil sink" calculation (run 4) produced the largest over-ocean annual mean interhemispheric

Table 5. Global Budget of CH_3Br Derived for Estimated Present-Day Atmosphere

Model Augmented by	5.5 ppt	4.7 ppt	τ, years
Sources and sinks, kT yr^{-1}			
Biomass burning	23.5	23.5	
Agro-industrial (with gasoline emissions of 5 kT yr^{-1})	51.9	51.9	
Soil sink	-43.5	-41.3	
Atmospheric loss	-104.5	-94.1	
Net oceanic flux	-31.8	-29.3	
Source required to balance model	104.4	89.3	
Ocean budget terms, kT yr^{-1}			
Oceanic physical/chemical loss	-101.1	-93.1	
In-situ Oceanic production	69.3	66.4	
Net flux into ocean	31.8	29.3	
CH3Br lifetime results			
τ wrt atmospheric losses			1.6
τ wrt oceanic destruction			2.1
τ wrt soil sink			3.7
Total atmospheric lifetime			0.7

wrt, with respect to.

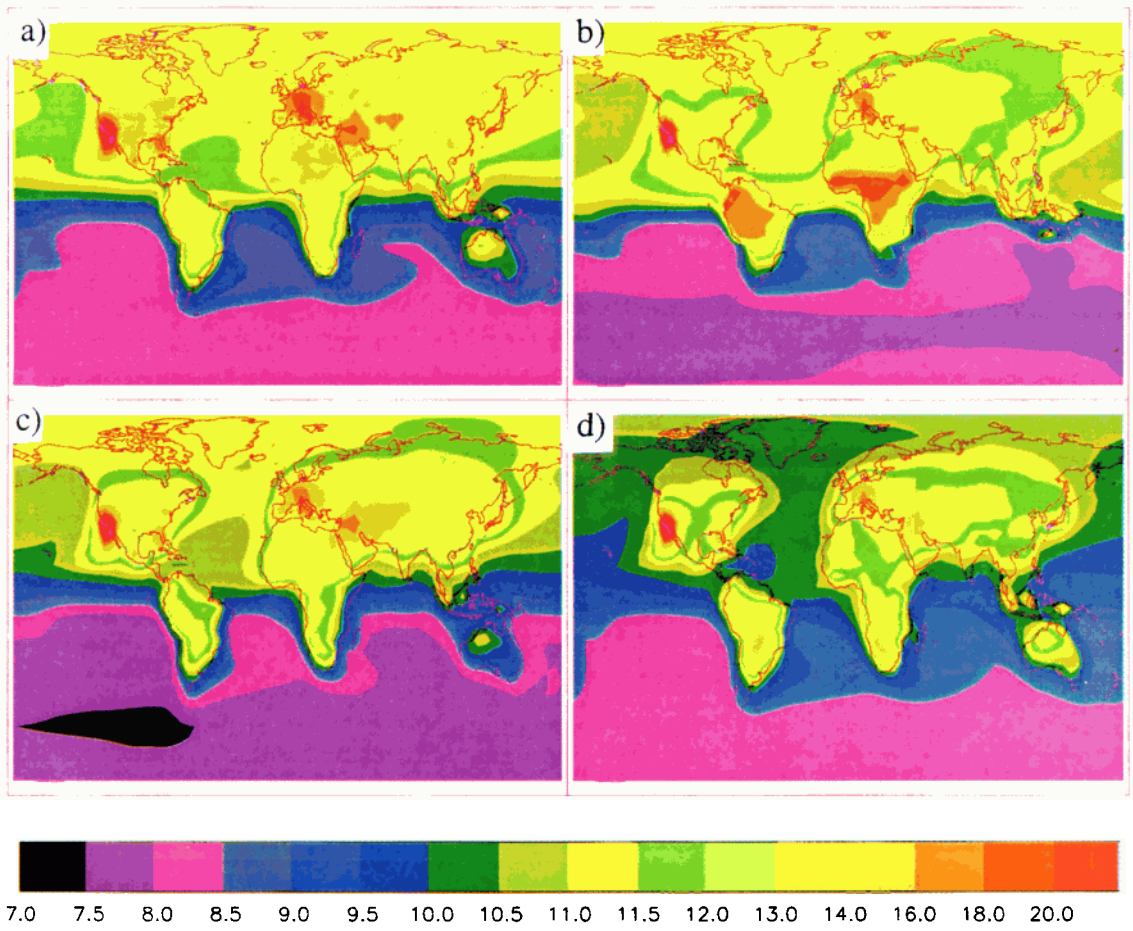

Plate 4. Modeled annual mean CH_3Br mixing ratio distribution for (a) run 5, larger additional source distributed over land surfaces in the ratio 50:50 N:S; (b) run 6, larger source confined to tropics; (c) run 7, smaller source, 50:50 N:S distribution; and (d) run 9, smaller source, 30:70 N:S distribution.

difference of all simulations, 3.6 ppt, while observations give a much lower value. This suggests that any additional source should be more evenly distributed between the hemispheres, if our other source/sink distributions are correct. A predominantly tropical land source distribution might also potentially satisfy this requirement.

4.4. Inclusion of Additional Net Source

To more closely constrain the additional CH_3Br net source (or sources) implied by the shortfall in the modeled mixing ratios, a second set of model runs examines the effects of a postulated additional source, with all other sources and sinks parameterized as in the base case (run 1). Since it is inconsistent with recent observations of oceanic saturation anomaly [*Lobert et al.*, 1995, 1996, 1997; *Moore and Webb*, 1996] that this additional source should originate from the open oceans, the CH_3Br source was distributed uniformly over land surfaces, with simplistic constraints being placed on latitudinal distribution. The coastal source (section 4.3) is neglected due to the localized nature of available observations [*Lobert et al.*, 1996]. We omit land areas poleward of 55°, since an initial exploratory calculation with latitudinally uniform emission gave disproportionately high mixing ratios in polar regions.

Two different net CH_3Br source strengths are considered. Runs 5 and 6 incorporate an additional 94.4 kT yr^{-1}, based on the comparison of the base case model results with both observational ocean transects. Run 5 distributes this source in the ratio 50:50 between the hemispheres and uniformly over land within each hemisphere (Table 3), avoiding assumptions about specific release processes. The source is confined to the tropical land surface (between 17.5°N and S) in run 6. The gasoline source in runs 7 through 9 is reduced to 5 kT yr^{-1}, to better represent the consensus of current understanding (e.g. J. Baker et al. and T. Chen et al. (manuscripts in preparation, 1998)). Runs 7 - 9 incorporate the resulting 10 kT yr^{-1} deficit into an additional net source of 89.3 kT yr^{-1}, which reflects the difference between the model and the Pacific data only. The hemispheric emission ratio of this source is 50:50 in run 7, 40:60 N:S in run 8, and 30:70 N:S in run 9. The resulting southern hemisphere mean emission rates are 1300 and 1800 g km^{-2} y^{-1} for runs 7 and 9, comparable to the maximum modeled annual mean agro-industrial emission rates (Plate 2a). Northern hemisphere mean emission rates are 350 g km^{-2} y^{-1} in run 7 and 590 g km^{-2} y^{-1} in run 9.

Modeled annual mean surface CH_3Br mixing ratio distributions for runs 5, 6, 7, and 9 are shown in Plate 4. Once again, a strong mixing ratio gradient is calculated for the equatorial region, and there is substantial longitudinal variability. While annual mean mixing ratios are again enhanced over northern hemisphere agro-industrial emission

regions, the gradients between these regions and oceanic areas are less pronounced than in runs 1 and 4 due to the significant increases in background mixing ratios resulting from the additional net source in runs 5 - 9. Conversely, longitudinal gradients in the southern hemisphere in runs 5 - 9 are increased with respect to runs 1 - 4, in response to the new land-based source.

Comparisons of the model results with observational data are summarized in Figures 6 - 9. The latitudinal distribution of the missing source can be roughly constrained, at least for this model, by comparing the simulated and observed values along the ocean transects (Figure 6) and at baseline monitoring stations (Figure 7), and the interhemispheric gradient (Figure 8, Table 4) and its seasonal cycle (Figure 9). Observational data sources are detailed in the figure captions.

Run 5, with the larger source estimate distributed equally between the hemispheres, overpredicts mixing ratios at most monitoring sites and in the northern Pacific on the ocean transect line. Better agreement between run 5 and observations is found in the tropical and Atlantic regions. When this same source is confined to the tropics (run 6), high-latitude and midlatitude station results agree with observations; however, tropical values are overpredicted. Note the sensitivity of the ocean transect results, especially those in the tropical Atlantic, to the location of the additional land-based source (Figure 6 and Plate 4). The overpredictions of mixing ratio (and lack of significant underpredictions) for both runs 5 and 6 suggest that the additional source applied in these cases (94.4 kT yr^{-1}) is too large. This source strength is based on an assessment of model results and observations on both ocean transects.

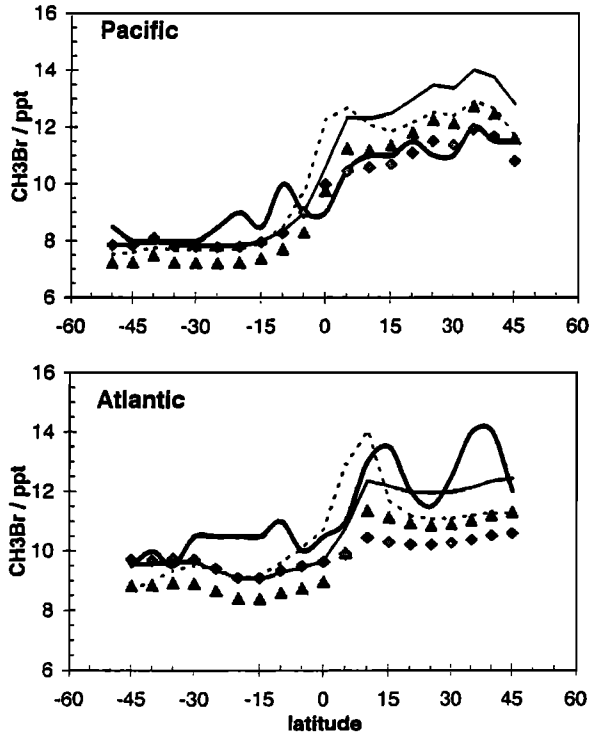

Figure 6. Comparison between atmospheric data of *Lobert et al.* [1995, 1996] (thick, smoothed line) and model results with additional net source. Runs 5 and 6 (larger source) are represented by thin lines while runs 7 and 9 (smaller source) are represented by symbols.

Though most of the monitoring sites referred to here are in the Pacific region where transect observations are lower, Mace Head, the lone Atlantic site, also shows overpredicted model mixing ratios. We note that the Atlantic transect observations were made in October and November, toward the end of the main biomass burning season in the southern hemisphere and the fumigation season in the northern hemisphere, while the Pacific transect was conducted in January and February, after what our model suggests is a period of relatively low variability and volume of emissions in each hemisphere. It is therefore possible that the Atlantic transect shows enhanced mean mixing ratios due to advection of air influenced by a variety of land-based sources, elevating it above "background" mixing ratios. The original data [*Lobert et al.*, 1995, 1996] does indeed show significantly more variability about the latitudinal mean over the Atlantic than over the Pacific.

Reduction of the additional net source to the level suggested by the Pacific transect alone reduces modeled CH_3Br mixing ratios to closely match most monitoring site observations for a 50:50 N:S additional source distribution (run 7), while run 9, with 30:70 N:S additional source partitioning tends to underrepresent the observational data in the north and produce overestimates in the south (Figure 7). Run 8 (with 40:60 N:S partitioning of the additional source) gives results intermediate between those of runs 7 and 9 at each location. The assumption of an equal distribution between the hemispheres (run 7), however, significantly overestimates the interhemispheric ratio (IHR) with respect to the observed value of 1.21±0.03 [*Wingenter et al.*, 1998].

Table 4 lists annual mean model interhemispheric ratio results calculated both over the modeled global ocean and between Alaska and New Zealand for direct comparability to the observed value. *Wingenter et al.* [1998] use observations from 71°N to 57°N in Alaska and between 37°S and 47°S on the New Zealand coast in their IHR assessment. We use the mean mixing ratios of four 5°×5° grid boxes in each region, approximating to transects between Barrow (71°N, 157°W) and Kodiak Island (57°N, 153°W) in Alaska, and between Aukland (37°S, 175°E) and Bluff (47°S, 169°E) in New Zealand (henceforth referred to as the "Alaska/New Zealand" assessment of the IHR). IHR values for Alaska/New Zealand are consistently higher than the area-weighted oceanic mean assessment. Extrapolation of the near-linear relationship between hemispheric partitioning of the lower additional source and modeled IHR (Figure 9) predicts that a 29:71 N:S source partitioning would best represent the observed Alaska/New Zealand IHR. These results suggest that the true proportion of the additional source originating in the southern hemisphere is somewhere between 50% and 70%, although significant variability in the source distribution may affect this result.

Model IHRs assessed between Alaska and Cape Grim (41°S, 145°E) are significantly lower than either the Alaska/New Zealand assessment or the mean ocean assessment. This may well be due to the relatively coarse model resolution employed here (5°×5°, monthly mean results), giving mixing ratios that are not necessarily representative of baseline (clean air) conditions at a coastal location such as Cape Grim. However, it also serves as a warning that IHR values assessed from observational data are not necessarily globally applicable. As an additional caution, we note that IHR does not depend solely on the ratio of

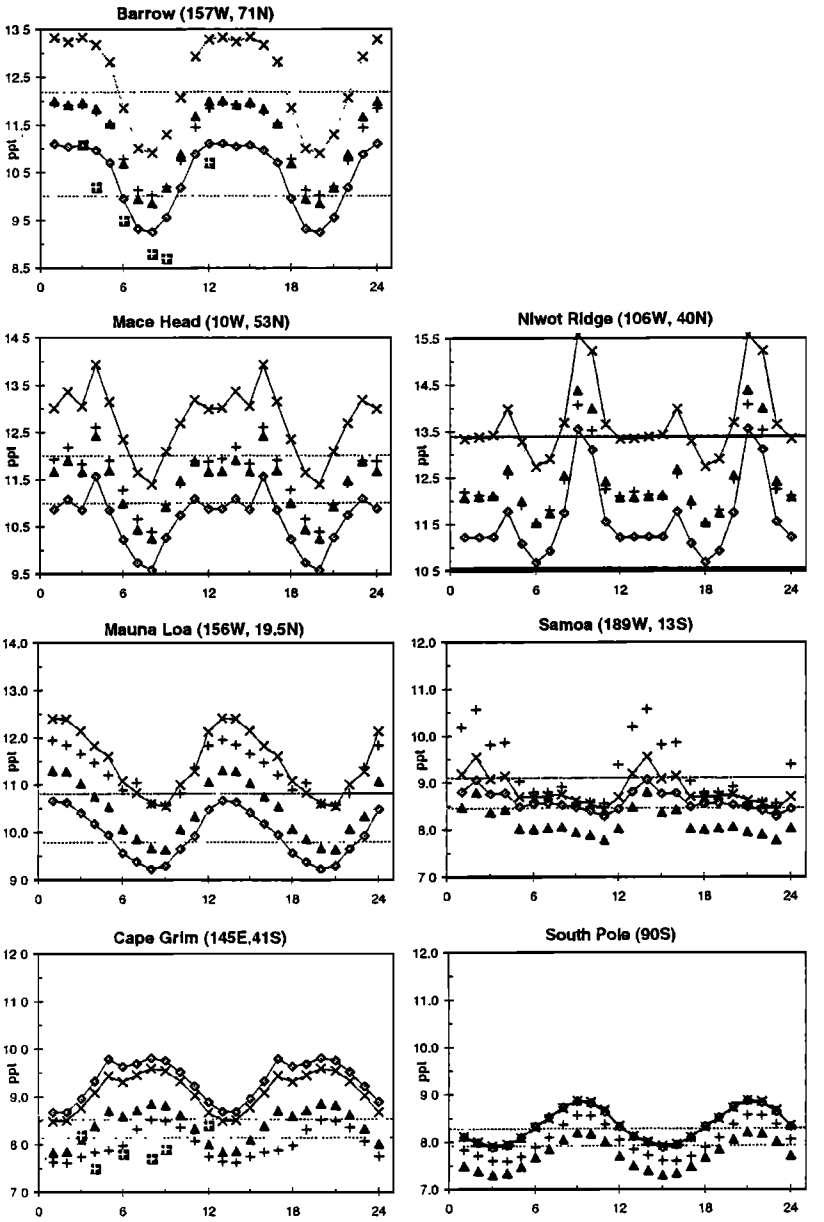

Figure 7. Seasonal cycles of modeled CH_3Br mixing ratio at selected monitoring site locations: crosses, run 5; plus signs, run 6; triangles, run 7; diamonds, run 9. Dashed horizontal lines represent the range of observations (S. Montzka, CMDL, personal communication, 1997; Mace Head values courtesy of D. Oram, UEA, personal communication, 1997). Large crossed squares are data of *Wingenter et al.* [1998].

emission between the hemispheres but also on distribution within each hemisphere. A trial simulation, with the larger source distributed evenly within each hemisphere equatorward of 55°, irrespective of land/ocean differences, gives an IHR of 1.26, compared to the IHR of 1.38 yielded by run 5. While this result has little bearing on the possible real-world location of the additional source, it does show that source (and probably sink) distribution is pertinent to the correct calculation of the IHR. This important issue cannot be addressed in zonal mean model or two-box model attempts to derive the relative importance of agro-industrial emissions to the global budget by comparison with the observed IHR.

If our analysis is correct and emissions from the southern hemisphere land surfaces account for at least one-half of the missing source, the most plausible explanation is a biogenic source. The underestimation of mixing ratios at Samoa by run 7 suggests that, while a tropically confined source is unlikely, tropical regions may well make a significant contribution. Uncertainties in the global biomass burning source estimate (total strength 24 kT yr^{-1}) are unlikely to be able to compensate for the full value of the missing source; also, if significant increases were to be made to the agro-industrial source, which originates predominantly in the northern hemisphere (Table 1), the interhemispheric ratio would increase, removing it further from observations. Methyl bromide and bromine in other forms is known to interact with and be incorporated into a wide variety of plant types [e.g., *Ellis et al.*, 1995; *Jeffers and Wolfe*, 1998]. CH_3Br emissions may occur as part of natural decomposition

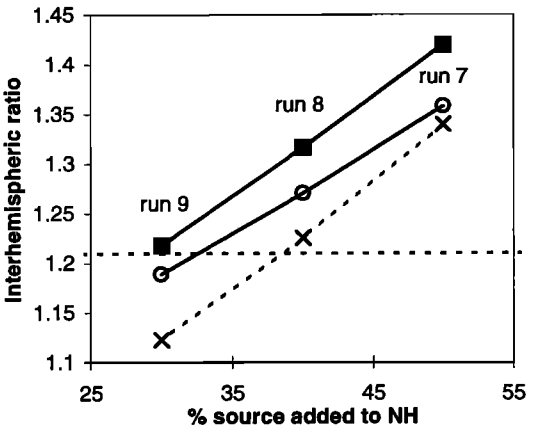

Figure 8. The relationship between modeled interhemispheric ratio to paritioning of the additional source between northern and southern hemispheres. Shown are, from the top, functions for the interhemispheric ratio calculated for Alaska/New Zealand, the mean of the hemispheric oceans, and Alaska/Cape Grim.

processes or at low but persistent levels, as part of transpiration. We note that the contribution of the southern hemisphere to global emissions of biogenic NMHCs is of the order of 50% [*Müller*, 1992], consistent with the hemispheric partitioning proposed here for the additional source of methyl bromide. Another possibility is that at least part of the estimated source may be due to emissions from intertidal or freshwater areas. Offshore coastal waters are, however, unlikely to make a substantial contribution to the magnitude of the missing source, given the low fluxes estimated by *Lobert et al.* [1995, 1996] from their observations.

The model results show distinct seasonal cycles at many of the stations (Figure 7), reflected by the seasonal variability in the interhemispheric ratio (Figure 9). In general, northern and southern sites show seasonal cycles that are out of phase with each other, so that the ratio between the hemispheres is highest in the early part of the year and lowest in August, in this model. The amplitude of the modeled seasonal cycle in IHR, ±28% of the mean, is comparable to the observations. The seasonal cycle predicted at Barrow, Alaska (Figure 6), is typical of observations of other trace constituents such as CFCs [*Montzka et al.*, 1996] and CO [*Novelli et al.* 1992 and references therein] in that it shows high, steady mixing ratios in the first few months of the year with a steep drop to a minimum in the third quarter, and is driven by transport. Niwot Ridge, Colorado, on the other hand, shows a calculated seasonal cycle almost indistinguishable from that produced by agriculture alone, due to its proximity to a major emission region (California) (r^2= 0.99 when compared to the results of a test run incorporating only the agricultural source and atmospheric interactions). It may be expected, however, that in reality, significant temporal variability might be observed at this site if winds from more northerly regions with lower mixing ratios and less agricultural influence are sampled on occasion.

Figure 10 shows seasonal altitudinal profiles for six locations from run 7. One notable feature is the surface enhancement in the Niwot Ridge profile, reflecting the tendency of continental interior mixing ratios to be greater than over-ocean values in results from this model. The effects are confined to the boundary layer, extending upward to only 1 km altitude (2.2 km above sea level at this site). The zonal mean cross section for November is shown in Figure 11 for the same run. Upward transport of CH_3Br from northern hemisphere midlatitude source regions and poleward transport at higher altitudes in the southern hemisphere are major features which persist throughout the year, despite the reduction in north/south gradient in the third quarter of the year (Figure 9). Seasonal profiles calculated for Samoa and Cape Grim (Figure 10) show slight increases in the upper troposphere due to this southward transport. Also persistent in the zonal mean cross section is the near-vertical nature of the mixing ratio isopleths in the equatorial region. The methane distribution generated by this model [*Müller and Brasseur*, 1995, Figure 9] duplicates this feature, which is due to strong equatorial convective upward transport (see also modeled isoprene and ozone, [*Müller and Brasseur*, 1995, Figures 11 and 28]. The effects of stratospheric destruction of CH_3Br reduce mixing ratios at the top of the profiles and the cross section.

5. Conclusions

The three-dimensional model of CH_3Br presented here yields a global distribution of atmospheric methyl bromide that exhibits latitudinal, longitudinal and altitudinal gradients as a result of transport and the source and sink climatologies developed in this study. We find no correlation between oceanic net production implied from observations and primary productivity. Ocean-atmosphere exchange is therefore constrained by an empirical function based on oceanic saturation anomaly observations. Mixing ratios modeled by including only known sources and sinks are on average 4.7 ppt lower than Pacific Ocean transect observations; if Atlantic Ocean observations are also considered, the mean difference is 5.5 ppt. A missing net source of 79 (94) kT yr^{-1} is implied by this model configuration. Downscaling of the gasoline-derived source by 10 kT yr^{-1} in line with recent estimates increases the missing source to 89 (104) kT yr^{-1}. Addition of the calculated missing source over land surfaces simulates

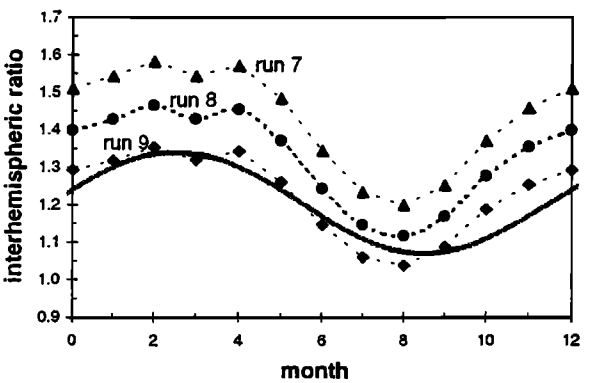

Figure 9. Seasonal cycles of modeled interhemispheric ratio between Alaska (71°N - 57°N) and New Zealand (37°S - 47°S) for runs 7, 8, and 9. Run 9 with 70% of the additional source emitted from the southern hemisphere appears to best match the observations, represented here by the sine function of *Wingenter et al.* [1998] (heavy line).

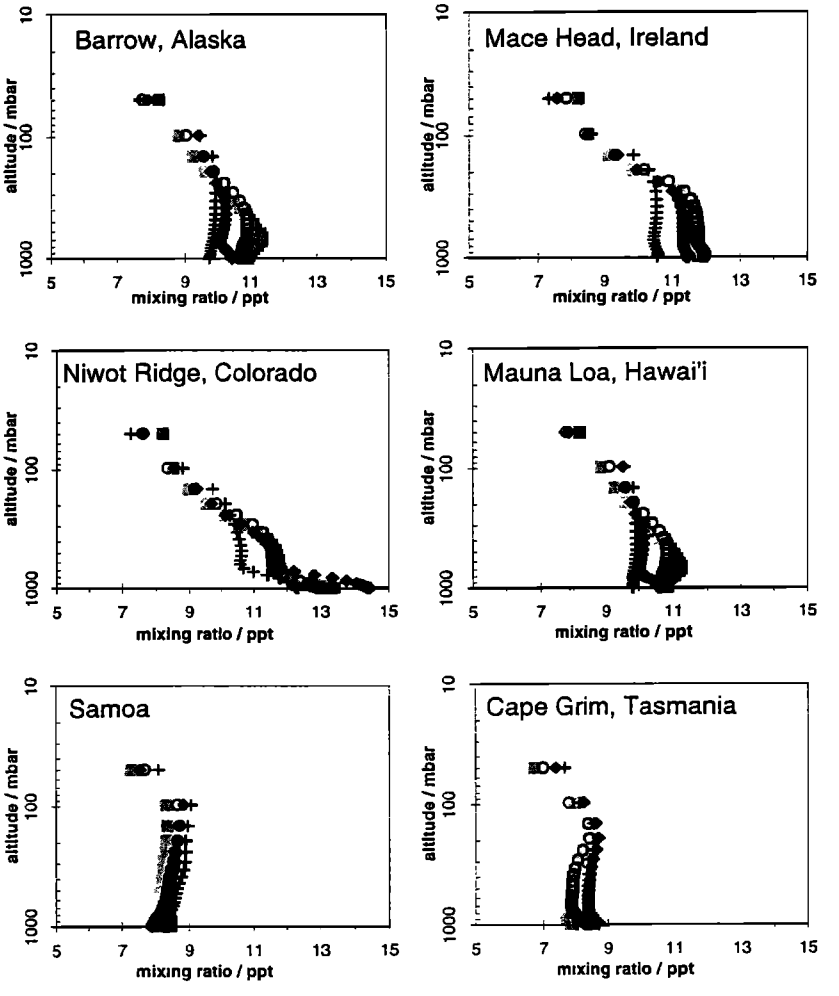

Figure 10. Modeled profiles for selected locations, run 7. Profiles are seasonal averages: squares, December/ January/February; circles, March/April/May; plus signs, June/July/August; diamonds, September/October/ November.

observations with a reasonable degree of success. We calculate a net global lifetime for methyl bromide of 0.7 year.

"Trial-and-error" experiments comparing the observed interhemispheric ratio and measured mixing ratios at several monitoring sites suggest that at least 50% but no more than

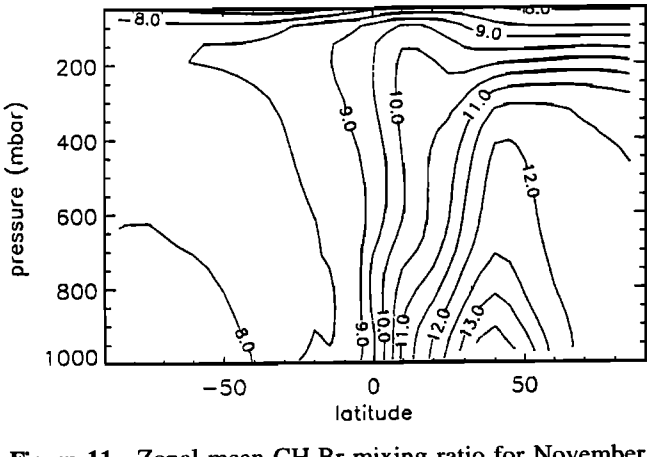

Figure 11. Zonal mean CH_3Br mixing ratio for November, run 7.

71% of the implied missing source may originate on or near land surfaces in the southern hemisphere. Revising the budget to include the missing source, about 30 % of the net source is due to agro-industrial emissions, while about 55% of the net land-based source is of unknown origin, though a continental biospheric component is strongly implied. The ocean constitutes a net sink of 29 - 32 kT yr^{-1}.

Refinement of the budget via inverse model calculations designed to further probe the distribution and magnitude of this source would require a 3-D model due to the longitudinally complex nature of the known source/sink distribution and the dependency of the IHR on both source/sink distribution and the precise location at which the IHR is assessed. Inverse model studies, however, also rely on wide spatial and seasonal observational coverage for their constraint. As the observational data set widens, an inverse study is becoming a more realistic endeavor. Model predictions of likely distribution of the net missing source may prove invaluable for guiding experimental research efforts to its eventual identification. Conversely, the more information gathered in the field regarding source processes for CH_3Br, the more realistic global modeling of its budget will become, especially as there may well be multiple source, and sink, processes yet uncharacterized.

Acknowledgments. This research was supported by NASA grant W-18-153. J.M. Lee-Taylor was partially supported by the NCAR Advanced Study Program. S. Doney received support in part from NASA SeaWiFS grant NAGW-3648. J.-F. Müller is supported by a grant of the Belgian Office for Scientific, Technical and Cultural Affairs. The National Center for Atmospheric Research is sponsored by the National Science Foundation. The authors are extremely grateful to S.A. Montzka (NOAA/CMDL) and D.E. Oram and S.A. Penkett (University of East Anglia) for permission to use their preliminary data. Discussions with E.A. Holland and S.M. Schauffler contributed greatly to the work; their comments on the manuscript are also gratefully acknowledged, as are those of two anonymous reviewers.

References

Anbar, A., Y.L. Yung, and F.P Chavez, Methyl bromide: ocean sources, ocean sinks, and climate sensitivity, *Global Biogeochem. Cycles, 10,* 175 - 190, 1996.

Anderson, S.O., and S. Lee-Bapty, Technology and economic assessment of methyl bromide uses, alternatives, and substitutes, in *Methyl Bromide: Its Atmospheric Science, Technology, and Economics*, United Nations Environment Programme, Nairobi, Kenya, June 1992.

Andreae, M.O., et al., Methyl halide emissions from savanna fires in southern Africa, *J. Geophys. Res., 101,* 23 603 - 23 613, 1996.

Antoine, D., J.-M., André, and A. Morel, Oceanic primary production 2. Estimation at global scale from satellite (coastal zone color scanner) chlorophyll, *Global Biogeochem. Cycles, 10,* 57 - 69, 1996.

Bates, T.S., K.C. Kelly, J.E. Johnson, & R.H. Gammon, Regional and seasonal variations in the flux of oceanic carbon monoxide to the atmsophere, *J. Geopyhys. Res., 100,* 23093 - 23,101, 1995.

Blake, D., and F.S. Rowland, Seasonal variation in the north/south gradient of methyl bromide and biomass burning emissions of methyl bromide, paper presented at 1995 Methyl Bromide State of the Science Workshop, Methyl Bromide Global Coalition, Monterey, Calif., June 5 - 7, 1995.

Blake, D.R., B. Sive, M. Zondlo, and F.S. Rowland, Estimated methyl bromide emissions from biomass burning (abstract), *Eos Trans. AGU 74*(43), Fall Meet. Suppl., 134, 1993.

Born, M., H Dörr, and I Levin, Methane consumption in aerated soils of the temperate zone, *Tellus, 42B,* 2-8, 1990.

Butler, J.H, and J.M. Rodriguez, Methyl bromide in the atmosphere, in *The Methyl Bromide Issue*, chapter 2, edited by C.H. Bell, N. Price, and B. Chakrabarti, John Wiley, New York, 1996.

Butler, J.H., J.W. Elkins, T.M. Thompson, and B.D. Hall, Oceanic consumption of CH_3CCl_3: Implications for tropospheric OH, *J. Geophys. Res., 96(D),* 22,347 - 22,355, 1991.

Cleveland, C.C., E.A. Holland, and J.C. Neff, Temperature regulation of soil respiration in an alpine tundra ecosystem, poster and abstract, paper presented at Front Range Meeting, AGU, Golden, Colo, Feb. 1993.

Couper, A.D. (Ed.), *The Times Atlas of the Oceans*, Van Nostrand Reinhold, New York, 1983.

Daniel, J.S., S.M. Schauffler, W.H. Pollock, S. Solomon, A. Weaver, L.E. Heidt, R.R. Garcia, E.L. Atlas, and J.F. Vedder, On the age of stratospheric air and inorganic chlorine and bromine release, *J. Geophys. Res., 101(D),* 16,757 - 16,770, 1996.

DeBruyn, W.J., and E.S. Saltzman, Diffusivity of methyl bromide in water, *Mar. Chem., 57,* 55 - 59, 1997.

DeMore, W.B., S.P. Sander, D.M. Golden, R.F. Hampson, M.J. Kurylo, C.J. Howard, A.R. Ravishankara, C.E. Kolb, and M.J. Molina, Chemical kinetics and photochemical data for use in stratospheric modeling, *JPL Pub. 94 - 26, Evaluation 11,* Jet Propul. Lab., Pasadena, Calif., 1994.

Elliott, S., and F.S. Rowland, Nucleophilic substitution rates and solubilities for methyl halides in seawater, *Geophys. Res. Lett., 20,* 1043 - 1046, 1993.

Ellis, J.R., D.M.H. Watson, G.E. Varval, and M.D. Jawson, Methyl bromide soil fumigation alters plant element concentrations, *Soil Sci. Soc. Am. J., 59,* 848 - 852, 1995.

Food and Agriculture Organization, 1989 FAO Production Yearbook, United Nations, Rome, Italy, 1990.

Gan, J., S.R. Yates, M.A. Anderson, W.F. Spencer, F.F. Ernst, and M.V. Yates, Effect of soil properties on degradation, and sorption of methyl bromide in soil, *Chemosphere, 29,* 2685 - 2700, 1994.

Granier, C., W.-M. Hao, G. Brasseur, and J.-F. Muller, Land use practices and biomass burning: Impact on the chemical composition of the atmosphere, in *Biomass Burning and Global Change*, edited by J.S. Levine, MIT Press, Cambridge, Mass., 1996.

Gschwend, P.M., J.K. MacFarlane, and K.A. Newman, Volatile halogenated organic compounds released to seawater from temperate marine microalgae, *Science, 227,* 1033 - 1035, 1985.

Guenther, A., et al., A global model of natural volatile organic compound emissions, *J. Geophys. Res., 100,* 8873 - 8892, 1995.

Holland, E.A., A.R. Townsend, and P.M. Vitousek, Variability in temperature regulation of CO_2 fluxes, and N mineralization from five Hawaiian soils: Implications for a changing climate, *Global Change Biol., 1,* 115 - 123, 1995.

Houghton, R.W., The relationship of sea-surface temperature to thermocline depth at annual and interannual timescales in the tropical Atlantic Ocean, *J. Geophys. Res., 96(C),* 15,173 - 15,185, 1991.

Jeffers, P.M. and N.L. Wolfe, Green plants: A terrestrial sink for atmospheric CH_3Br, *Geophys. Res. Lett., 25,* 43-46, 1998.

Johnson, J.E., The lifetime of carbonyl sulfide in the troposphere, *Geophys. Res. Lett., 8,* 938 - 940, 1981.

Kalnay, E., et al., The NCEP/NCAR reanalysis project, *Bull. Am. Meteorol. Soc., 77,* 437 - 471, 1996.

Khalil, M.A.K., R.A. Rasmussen, and R. Gunawardena, Atmospheric methyl bromide: trends and global mass balance, *J. Geophys. Res., 98,* 2887 - 2896, 1993.

King, D.B., and E.S. Saltzman, Removal of methyl bromide in coastal seawater: Chemical and biological rates, *J. Geophys. Res., 102(C),* 18,715 - 18,721, 1997.

King, D.B., C. Plinis, and E.S. Saltzman, Measurement of the total degradation rate of methyl bromide in seawater (abstract), *Eos Trans. AGU, 76,* Spring Meet. Suppl., S162, 1995.

Lal, S., R. Borchers, P. Fabian, P.K. Patra, and B.H. Subbaraya, Vertical distribution of methyl bromide over Hyderabad, India, *Tellus, 46B,* 373 - 377, 1994.

Levitus, S., Climatological atlas of the world ocean, *NOAA Prof. Pap., 13,* U.S. Govt Print. Off., Washington D.C., 1982.

Li, Y.-H., T.-H. Peng, W.S. Broecker, and H.G. Östlund, The average vertical mixing coefficient for the oceanic thermocline, *Tellus, 36B,* 212 - 217, 1984.

Lobert, J.M., J.H. Butler, S.A. Montzka, L.S. Geller, R.C. Myers, and J.W. Elkins, A net sink for atmospheric CH_3Br in the east Pacific Ocean, *Science, 267,* 1002 - 1005, 1995.

Lobert, J.M., J.H. Butler, L.S. Geller, S.A. Yvon, S.A. Montzka, R.C. Myers, A.D. Clarke, and J.W. Elkins, BLAST94: Bromine latitudinal air/sea transect 1994, Report on oceanic measurements of methyl bromide and other compounds, *NOAA Tech. Memo. ERL CMDL-10,* NOAA, Boulder, Colo., Feb. 1996.

Lobert, M., S.A. Yvon-Lewis, J.H. Butler, S.A. Montzka, and R.C. Myers, Undersaturations of CH_3Br in the Southern Ocean, *Geophys. Res. Lett., 24,* 171, 1997.

Manö, S, and M.O. Andreae, Emission of methyl bromide from biomass burning, *Science, 263,* 1255 - 1257, 1994.

Methyl Bromide Global Coalition, Methyl bromide: Annual production and sales for the years 1984 - 1992, Grant Thornton Accountants, Washington, D.C., June 1994.

Methyl Bromide Industry Panel / Chemical Manufacturers Association (MBIP/CMA), Methyl Bromide Annual Production and Sales for the Years 1984 - 1990, Washington, D.C., February 1992.

Miller, B.R., and R.F. Weiss, Methyl bromide distributions in the surface ocean and atmosphere of the eastern Pacific off southern

California, paper presented at 1995 Methyl Bromide State of the Science Workshop, Methyl Bromide Global Coalition, Monterey, Calif., June 5 - 7, 1995.

Montzka, S.A., R.C. Myers, J. Harris, and R. Norton, Methyl bromide at a rural site in the southeastern U.S. (abstract), *Eos Trans. AGU, 75,* Fall Meet. Suppl., F110, 1994.

Montzka, S.A., J.H. Butler, R.C. Myers, T.M. Thompson, T.H. Swanson, A.D. Clarke, L.T. Lock, and J.W. Elkins. Decline in the tropospheric abundance of halogen from halocarbons: Implications for stratospheric ozone depletion, *Science, 272,* 1318 - 1322, 1996.

Moore, R.M., and M. Webb, The relationship between methyl bromide and chlorophyll α in high latitude ocean waters, *Geophys. Res. Lett., 23,* 2951 - 2954, 1996.

Müller, J.-F., Geographical distribution and seasonal variation of surface emissions and deposition velocities of atmospheric trace gases, *J. Geophys. Res., 97,* 3787 - 3804, 1992.

Müller, J.-F., and G. Brasseur, IMAGES: A three-dimensional chemical transport model of the global atmosphere, *J. Geophys. Res., 100,* 16,445 - 16,490, 1995.

Novelli, P.C., P. Steele, and P.P. Tans, Mixing ratios of carbon monoxide in the troposphere, *J. Geophys. Res., 97,* 20,731 - 20,750, 1992.

Olson, J. S., J. A. Watts, and L. J. Allison, Carbon in live vegetation of major world ecosystems, *DOE/NBB Rep. TR004,* Dep. of Energy, Oak Ridge Natl. Lab., Oak Ridge, Tenn., 1983.

Olson, J. S., J. A. Watts, and L. J. Allison, Major world ecosystem complexes ranked by carbon in live vegetation, A data base, *Rep. ORNL-5862,* 164 pp., Oak Ridge Natl. Lab., Oak Ridge, Tenn., 1985.

Oremland, R., P. Visscher, J. Guidetti, T. Connell, and L. Miller, Degradation of methylbromide (MeBr) in shoreline microbial mats of Mono Lake, CA, paper presented at 1995 Methyl Bromide State of the Science Workshop, Methyl Bromide Global Coalition, Monterey, Calif., June 5 - 7, 1995.

Penkett, S.A., Methyl bromide, Scientific assessment of ozone depletion: 1994, chap. 10, *Rep.37,* Global Ozone Res. and Monit. Proj., World Meterol. Organ., Geneva, Switzerland, 1995.

Pilinis, C., D.B. King, and E.S. Saltzman, The oceans: A source or a sink of methyl bromide?, *Geophys. Res. Lett., 23,* 817 - 820, 1996.

Prather, M.J., Atmospheric lifetimes of HCFCs and HFCs: Current estimates and uncertainties, paper presented at the Workshop on the Atmospheric Degradation of HCFCs and HFCs, NASA/NOAA/ AFEAS, Boulder, Colo., November 17 - 19, 1995.

Prinn, R.G., R.F. Weiss, B.R. Miller, J. Huang, F.N. Alyea, D.M. Cunnold, P.J. Fraser, D.E. Hartley, and P.G. Simmonds, Atmospheric trends and lifetime of CH_3CCl_3 and global OH concentrations, *Science, 269,* 187 - 192, 1995.

Reeves, C.E., and S.A. Penkett, An estimate of the anthropogenic contribution to atmospheric methyl bromide, *Geophys. Res. Lett., 20,* 1563 - 1566, 1993.

Rolston, D.E., and R.D. Glauz, Comparisons of simulated with measured transport and transformation of methyl bromide in soils, *Pestic. Sci., 13,* 653 - 664, 1982.

Scarrat, M.G., and R.M. Moore, Production of methyl halides by anexic cultures of the marine diatom *Phaeodactylum tricornutum* (abstract), *Eos Trans. AGU, 76,* Spring Meet. Suppl., S168, 1995.

Schauffler, S.M., L.E. Heidt, W.H. Pollock, T.M. Gilpin, J.F. Vedder, S. Solomon, R. A. Lueb, and E.L. Atlas, Measurements of halogenated organic compounds near the tropical tropopause, *Geophys. Res. Lett., 22,* 2567 - 2570, 1993a.

Schauffler, S.M., W.H. Pollock, and E.L. Atlas, Methyl bromide measurements taken from the marine boundary layer and during the 1991 - 1992 AASE II flights, in *Proceedings of the Methyl Bromide State of the Science Workshop,* Methyl Bromide Global Coalition/NASA, October 28, 1993, SPA Inc., Washington D.C, 1993b.

Schauffler, S.M., E.L. Atlas, F. Flocke, R.A. Lueb, V. Stroud, and W. Travnicek, Measurements of bromine containing organic compounds at the tropical tropopause, *Geophys. Res. Lett., 25,* 317 - 320, 1998.

Seiber, J.N., K. Dowling, J. Lenoir, J.E. Woodrow, C. Wujcik, and M. Gillis, Methyl bromide volatilization and downwind fate, paper presented at 1995 Methyl Bromide State of the Science Workshop, Methyl Bromide Global Coalition, Monterey, Calif., June 5 - 7, 1995.

Shea, D.J., K.E. Trenberth, and R.W. Reynolds, A global monthly sea-surface temperature climatology, *NCAR Tech. Note NCAR/TN-345+STR,* 167 pp., Natl. Center for Atmos. Res., Boulder, Colo., 1990.

Shea, D.J., K.E. Trenberth, and R.W. Reynolds, A global monthly sea surface temperature climatology, *J. Clim., 5,* 987-1001, 1992.

Shorter, J.H., C.E. Kolb, P.M. Crill, R.A. Kerwin, R.W. Talbot, M.E. Hines, and R.C. Harriss, Rapid degradation of atmospheric methyl bromide in soils, *Nature, 377,* 717 - 719, 1995.

Singh, H.B., and M. Kanakidou, An investigation of the atmospheric sources and sinks of methyl bromide, *Geophys. Res. Lett., 20,* 133 - 136, 1993.

Singh, H.B., L.J. Salas, and R.E. Stiles, Methyl halides in and over the eastern Pacific (40°N-32°S), *J. Geophys. Res., 88,* 3684 - 3690, 1983.

Solomon, S., M. Mills, L.E. Heidt, W.H. Pollock, and A.F. Tuck, On the evaluation of ozone depletion potentials, *J. Geophys. Res., 97,* 825 - 842, 1992.

Stamnes, K., S.C. Tsay, W.J. Wiscombe, and K. Jayaweera, Numerically stable algorithm for discrete-ordinate-method radiative transfer in multiple scattering and emitting layered media, *Appl. Opt., 27,* 2502 - 2509, 1988.

Sturges, W.T., C.W. Sullivan, R.C. Schnell, L.E. Heidt, and W.H. Pollock, Bromoalkane production by Antarctic ice algae, *Tellus, 45B,* 120 - 126, 1993.

United Nations Environment Programme, Report of the ninth meeting of the parties to the Montreal protocol on substances that deplete the ozone layer, *UNEP/OzL.Pro.9/12,* www.unep.org/unep/secretar/ozone/ reports.htm, Nairobi, Kenya, September 25, 1997.

U.S. Department of Agriculture, Agricultural chemical usage 1990 vegetables summary, *Rep. Ag Ch 1 (91),* Natl. Agric. Stat. Serv., Washington, D.C., 1991.

Wanninkhof, R., Relationship between wind speed and gas exchange over the ocean, *J. Geophys. Res., 97,* 7373 - 7382, 1992.

Wingenter, O.W., C.J.-L. Wang, D.R. Blake, and F.S. Rowland, Seasonal variation of tropospheric methyl bromide concentrations: constraints on anthropogenic input, *Nature,* in press, 1998.

Yagi, K., J. Williams. N.-Y. Wang, and R.J. Cicerone, Agricultural soil fumigation as a source of atmospheric methyl bromide, *Proc. Natl. Acad. Sci. USA, 90,* 8420 - 8423, 1993.

Yagi, K., J. Williams. N.-Y. Wang, and R.J. Cicerone, Atmospheric methyl bromide (CH_3Br) from agricultural soil fumigations, *Science, 267,* 1979 - 1981, 1995.

Yvon, S.A., and J.H. Butler, An improved estimate of the oceanic lifetime of atmospheric CH_3Br, *Geophys. Res. Lett., 23,*.53 - 56, 1996.

Yvon-Lewis, S.A., and J.H. Butler, The potential effect of oceanic biological degradation on the lifetime of atmospheric CH_3Br, *Geophys. Res. Lett., 24,* 1227 - 1230, 1997.

G. Brasseur, and J.M. Lee-Taylor, Atmospheric Chemistry Division, National Center for Atmospheric Research, P.O. Box 3000, Boulder, CO 80307. (e-mail: julial@ucar.edu)

S.C. Doney, Climate and Global Dynamics Division, National Center for Atmospheric Research, P.O. Box 3000, Boulder, CO 80307.

J.-F. Müller, Belgian Institute for Space Aeronomy, 3 Avenue Circulaire, 1180 Brussels, Belgium.

(Received November 19, 1997; revised February 16, 1998; accepted March 16, 1998.)